12-2008

Fabrication and Optical Properties of Noble Metal Nanostructures

Mark Kinnan
Clemson University, mark@saponico.com

FABRICATION AND OPTICAL PROPERTIES OF NOBLE METAL NANOSTRUCTURES

A Dissertation
Presented to
the Graduate School of
Clemson University

In Partial Fulfillment
of the Requirements for the Degree
Doctor of Philosophy
Chemistry

---

by
Mark Keller Kinnan
December 2008

Accepted by:
George Chumanov, Committee Chair
Julia Brumaghim
Kenneth Christensen
Stephen Creager

ABSTRACT

Experimental and theoretical results are presented in Chapters 2, 3, and 4 on the effects of dielectric medium, particle size, and interparticle distance, respectively, on plasmon coupling in two-dimensional arrays of silver nanoparticles. The arrays were fabricated via the self-assembly of single crystal particles from c.a. 46 nm to 287 nm on PVP-modified glass substrates. Spin-coated poly(methylmethacrylate) layers were used to immobilize the particles and prevent their surface aggregation. Varying the thickness of the PMMA layer made it possible to change the average dielectric medium between the particles. UV-Visible spectra of different arrays were compared to the corresponding electron microscope images. It was found that increasing the dielectric function of the medium surrounding the particles promoted the coherent plasmon coupling of the particles. It was also observed that increasing the size of the particles in arrays resulted in red shifting and broadening of the coupled plasmon peak. The peak position against the particle size exhibited a linear trend, providing the possibility to adjust a lambda maximum by selecting an appropriate particle size. Decreasing the interparticle distance resulted in spectral shifting and broadening of the plasmon peak and affected the intensity and sharpness of the peaks. Smaller particles shifted to the red spectral range, where as larger particles shifted in the opposite direction upon decreasing the interparticle distance.

The phenomenon known as Surface Enhanced Raman Spectroscopy (SERS) is presented in Chapter 5. An analysis of spectra from 20 different molecules adsorbed on SERS substrates revealed competitive Raman enhancement from different types of

molecules simultaneously present on the surface. The observed SERS behavior could not be explained using local field enhancement or charge-transfer models. A different SERS mechanism is proposed based on plasmon-induced electronic coupling between the oscillating electrons in the metal and the electronic system of adsorbed molecules.

Chapter 6 continues a discussion of SERS but introduces a new substrate based on the low-pressure air plasma reduction of silver compounds to produce porous nanostructured surfaces. This method is advantageous because substrates are easy to prepare and the silver surface is inherently clean for the adsorption of molecules. Silver chloride was found to be the best compound to make reproducible and stable SERS substrates. SERS activity of the substrates was tested using L-tryptophan, 4-mercaptobenzoic acid, and adenine.

DEDICATION

This dissertation is dedicated to everyone that believed in me, supported me, or had an impact on me during my time at Clemson University.

ACKNOWLEDGMENTS

First and foremost, I must thank my advisor George Chumanov for giving me the opportunity to work in his lab. The knowledge and experience I have gained is invaluable, and I hope to build on all he has taught me as I pursue future opportunities. I would also like to thank all the Chumanov group members (past and present), other research group members, and my committee for the fruitful discussions over the years.

I am also grateful for the financial support from the United States Department of Energy (grant No. DE-FG02-06ER46342) because none of this research could have been accomplished without their support. Additional funding came from the Belarusian Republican Foundation for Fundamental Research, grant No. F07M-228.

TABLE OF CONTENTS

Table of Contents (Continued)

Page

Table of Contents (Continued)

Page

LIST OF TABLES

LIST OF FIGURES

List of Figures (Continued)

Figure Page

List of Figures (Continued)

Figure Page

List of Figures (Continued)

Figure Page

CHAPTER ONE

INTRODUCTION

As technology advances and devices enter nanodimensions, it is imperative to understand the science and properties of materials at this scale. Nanosize materials exhibit properties that are not observed in either solution or macroscopic phases. In silver nanoparticles (SNPs), light can excite the collective oscillations of the free electron density, also known as plasmon resonances.[1] The excitation of plasmon resonances is a unique property of SNPs and represents the most efficient mechanism by which light interacts with matter. It has been demonstrated in our laboratory that the optical cross section of SNPs is 10 times larger than the geometric cross section.[2] Silver nanoparticles must be large enough (c.a. 10 or more atoms) to have free electron density [3], but be small enough (less than the wavelength of visible light) that the optical properties change with particle size, shape, and local environment.[1, 4-8] The optical properties of SNPs make them attractive for a variety of optical and photonic applications such as biosensors [9], optical filters [10], plasmonic waveguides [11], and substrates for surface-enhanced Raman spectroscopy [12, 13].

As particles grow in size, the plasmon peak grows in intensity and shifts to longer wavelengths. The plasmon bandwidth of SNPs also increases with the size of the particles due to the excitation of multipole (dipolar, quadrupolar, octupolar, hexadecapolar, etc.) modes within the SNPs. The excitation of these modes is a result of the phase retardation of the incident field.[1, 14-16] When particles are small as compared to the wavelength of incident radiation, the entire particle experiences the same

phase of the incident radiation. As the particle dimensions become larger, the different areas experience different phases resulting in the formation of multiple plasmon modes. The increase in bandwidth is also a result of radiative damping of the plasmon oscillations in the nanoparticle. The efficient emission (scattering) of photons reduces the lifetime of the plasmon oscillations and broadens the plasmon band.

The excitation of plasmon resonances in SNPs produces a local electromagnetic field that extends from the particle surface and into the surrounding environment. This field is 'enhanced' as compared to the incident field and is a concentration of the incident field around the particle. It was experimentally demonstrated in our laboratory that the local electromagnetic field extends approximately ~40 nm from c.a. 84 ± 5 nm diameter SNPs.[17] Two-dimensional assemblies of SNPs exhibit new optical properties not observed for particles in suspension. In 2D assemblies of closely spaced particles, the local electromagnetic fields from SNPs can overlap with neighboring particles to result in plasmon coupling. The plasmon coupled peak depends on the particle size and shape, interparticle spacing, nature of the supporting substrate, and local dielectric environment. [5, 18-20] The effects of these parameters on plasmon coupling in 2D arrays of SNPs have been studied experimentally [7, 19, 21-27]. Theoretical calculations have found that coupling occurs when the interparticle distance is comparable to the nanoparticle diameter.[17, 19] It has been determined that as the dielectric environment increases around the particles, the plasmon coupled peak shifts to longer wavelengths.[20, 28] There are, however, differences in the literature regarding the direction of shift of the plasmon coupled peak upon changes in the interparticle distance. The majority report a

red spectral shift upon decrease of the interparticle distance where as others show blue spectral shifting of the plasmon mode.[7] This topic will be discussed further in CHAPTER IV.

In our laboratory, 2D arrays of SNPs resulted in a sharp band in the blue spectral region of the extinction spectra, corresponding to a coherent plasmon mode.[19] No other experimental reports of the sharp band appear in the literature, but the sharp band has been theoretically calculated by other groups.[29-31] I recently completed a thorough investigation related to the effects of surrounding dielectric medium, particle size, and interparticle distance on the coherent plasmon coupling in 2D arrays. It was found that increasing the dielectric function of the medium surrounding the particles promoted the coherent plasmon coupling of the particles. There was also a linear correlation between the increased size of the nanoparticles and the corresponding red spectral shift of the coherently coupled plasmon peak. Decreasing the interparticle distance resulted in either a red or blue spectral shift depending on the size of the nanoparticle. Experimental and theoretical results are presented on the effects of dielectric medium (Chapter 2), particle size (Chapter 3), and interparticle distance (Chapter 4) on plasmon coupling in 2D arrays of silver nanoparticles. The work presented in these chapters will be submitted to the *Journal of Physical Chemistry C* as a series of three papers.

Surface plasmons are an important property of SNPs and are also responsible for the phenomenon known as Surface Enhanced Raman Spectroscopy (SERS). Normal Raman is a weak process where only 1 out of 1 x 10^7 photons is Raman scattered.[32]

However, bringing a Raman-active molecule near a nanostructured noble metal surface such as gold or silver could result in the enhancement of the Raman scattering.[33] Ever since this discovery in 1974, SERS has developed into a widely researched field with more than 6000 SERS related papers. It has been found that an important requirement for the generation of SERS is that the noble metal surface must have roughness features on the scale of 50 – 200 nm in order to support surface plasmons.[34] Nanostructured features can be achieved in many ways such as oxidation-reduction cycles on an electrode surface [33], adsorption of metal colloids onto a surface [35], vacuum deposition of metals onto dielectric materials [36, 37], and metal nanostructures produced by lithography [38].

A long standing question of SERS is the mechanism by which the enhancement takes place. Numerous theories have been suggested, and the two predominant explanations are the local field enhancement mechanism (LFEM) and the chemical enhancement mechanism (CEM). In LFEM, the excitation of surface plasmons in the nanostructured features of the metal results in an 'enhanced' local electromagnetic field.[34, 39-44] The incident field together with the local electromagnetic field from the nanostructure increases the rate of Raman excitation of the molecules. An important feature of LFEM is that molecules do not need to be adsorbed to the metal surface but must be within the 'enhanced' local electromagnetic field from the nanostructures.

The CEM requires a specific interaction between the adsorbed molecules and the metal surface that could lead to the increased polarizability of the molecule. The increased polarizability can occur with the formation of a charge transfer complex

(CTC).[45-51] It is important to differentiate between two different types of CTCs: ground state CTC and excited state CTC.[42] Ground state CTC occurs when a chemical bond (covalent or ionic) is forged between the metal and molecule in the absence of light and charge is transferred from the metal to the molecule or vice versa. When the complex is formed under incident light, it is referred to as an excited state CTC. Both of these complexes have a larger polarizability than the free molecules and could result in the resonant transition in the visible region that leads to 'resonance' enhanced Raman scattering.

Acquiring SERS measurements from 'real world' samples is challenging due to interference from the sample matrix. Other molecules in the matrix compete with molecules of interest for the SERS substrate. In order to develop substrates to measure molecules of interest and minimize interference from the sample matrix, a firm understanding of the SERS mechanism is required. In model SERS studies, only one type of analyte is usually investigated at a time. Several papers have discussed measuring different molecules on a SERS substrate, but no detailed investigation has been published.[52-55] Before real world samples can be analyzed, it is important to understand the SERS signal when different molecules are simultaneously present on the SERS substrate.

In our laboratory, we developed a substrate that can be used to study two different molecules on the same substrate at the same time in a controlled manner. Silver nanoparticles were immobilized to a silver metal film with one kind of molecule to make the SERS substrate, and then a second type of molecule was added. I tested 20 different

molecules on the substrate and discovered that neither LFEM nor CEM could explain the experimental results. A different SERS mechanism named *plasmon-induced electronic coupling* was suggested based on the analysis of the SERS spectra. The analysis of the spectra revealed competitive Raman enhancement between the molecules used to adsorb the SNPs and the second molecules that were added. This mechanism considers the direct interaction of the oscillating electrons of the plasmon resonances with the adsorbed molecules. Many papers have suggested that surface plasmons can interact with molecules adsorbed to metal surfaces but this interaction was not directly linked to the SERS mechanism.[56-62] In the proposed model, the collective oscillations of electrons (surface plasmons) that are generated on the metal surface penetrate from the metal and into the electronic system of the adsorbed molecules. This results in an increased polarizability of the molecule and, consequently, an increase in Raman scattering. A detailed discussion of this SERS mechanism is presented in Chapter 5. The work presented in this chapter was published in the *Journal of Physical Chemistry C* (Copyright 2007, American Chemical Society). The citation for this manuscript is:

> Kinnan, M.K. and G. Chumanov. *Surface enhanced Raman scattering from silver nanoparticle arrays on silver mirror films: Plasmon-induced electronic coupling as the enhancement mechanism.* Journal of Physical Chemistry C, 2007. **111**(49): p. 18010-18017.

SERS has become a powerful technique; however, it is not a standard analytical tool yet due to the incomplete understanding of the enhancement mechanism, as was mentioned above, and the lack of highly reproducible substrates. There are numerous types of SERS substrates such as metal island films, electrochemically roughened

electrodes, or metal nanoparticle aggregates but the problem with these substrates is that they do not yield reproducible SERS. SERS from the same molecule must be reproducible from substrate to substrate as well as from different areas of the same substrate in order to achieve quantitative SERS measurements. It has been shown that substrates produced with electron beam lithography have increased signal reproducibility because of the precise control of the surface morphology.[63, 64] However, this type of substrate is costly and time consuming to fabricate. Two companies, Real-Time Analyzers [65] and D3 Technologies [66], have developed substrates that they believe are reproducible enough to be used at a quantitative level, although the price tag of $100 per-single-use substrate remains too high for practical use.

I developed a SERS substrate in an attempt to overcome the problem of substrate irreproducibility. The use of low-pressure air plasma to reduce silver compounds yielded nanostructured substrates that resulted in reproducible SERS signals. The method is advantageous because substrates are easy to prepare and the silver metal surface is inherently clean for the adsorption of molecules. A detailed discussion of this SERS substrate is presented in Chapter 6. The work presented in this chapter was published in *Applied Spectroscopy* (Copyright 2008, Optical Society of America). This work was also featured as the cover story for the July issue. The citation for this manuscript is:

Kinnan, M.K., A. Kumbhar, and G. Chumanov. *Plasma reduction of silver compounds for fabrication of surface-enhanced Raman scattering substrates.* Applied Spectroscopy, 2008. **62**(7): p. 721-726.

In addition to the studies discussed above, I collaborated in projects that involved the use of SNPs in textile and optical applications. SNPs were attached to PVP modified polyester fibers followed by further modification with a PMGA coating to increase the surface area and hydrophobicity of the fibers. Fabrics made of these fibers exhibited ultrahydrophobicity. The citation for this manuscript is:

> Rarnaratnam, K., S.K. Iyer, M.K. Kinnan, G. Chumanov, P. Brown, and I. Luzinov. *Ultrahydrophobioc textiles: Lotus approach.* AATCC Review, 2008. **8**(1): p. 42-48.

In a separate study, SNPs were assembled into 2D chains and the effect of polarization on the optical properties of the chains was investigated. The citation of this manuscript is:

> Zdyrko, B., M.K. Kinnan, G. Chumanov, and I. Luzinov. *Fabrication of optically active flexible polymer films with embedded chain-like arrays of silver nanoparticles.* Chemical Communications, 2008(11): p. 1284-1286.

These two papers are not discussed in this dissertation.

CHAPTER TWO

PLASMON COUPLING IN TWO-DIMENSIONAL ARRAYS OF SILVER NANOPARTICLES: 1. EFFECT OF THE DIELECTRIC MEDIUM

INTRODUCTION

Optical properties of silver nanoparticles (SNPs) are determined by the excitation of the plasmon resonances that are the collective oscillations of the free electron density.[1] The optical excitation of plasmon resonances in SNPs represents the most efficient mechanism by which light interacts with matter. By varying the particle size, shape, and surrounding dielectric medium the plasmon resonance can be tuned across the near-UV, visible, and near-infrared spectral range. The high efficiency for interaction with light, tunability of the optical resonance, as well as photochemical robustness makes SNPs attractive for applications in optical filters[67], plasmonic waveguides[11], substrates for surface-enhanced spectroscopies[7, 12, 13], and biosensors[8, 9].

The excitation of plasmon resonances produces an electromagnetic field localized around SNPs that is enhanced as compared to the incident field. Evanoff *et al.* reported that the local electromagnetic field extends approximately 40 nm from the surface of 84 nm diameter particles.[17] When several particles are put into close proximity so that the local fields associated with electron oscillations in individual particles overlap, the system undergoes plasmon coupling and new plasmon modes result. The plasmon coupling was observed in 2D arrays of SNPs as a sharp band in the blue spectral range of the extinction spectra representing a coherent plasmon mode.[19] Drying of these arrays changed the refractive index of the medium between the particles from that of water (1.33) to that of air (1) and resulted in a loss of the sharp band. Additionally, the drying

lead to the aggregation of the SNPs due to the forces associated with the surface tension of water as it dries.[68] Malynych *et al.* reported that the sharp band was preserved when the arrays were embedded into the poly(dimethylsiloxane) polymer matrix.[68] Even though embedding the SNPs into polymer matrixes proved to stabilize SNPs from aggregation, the particles are covered with a polymer and their surface is not accessible to the environment – a feature desired for sensing applications of these arrays. It was previously shown that the coupled SNP arrays that are not embedded into polymers can be used for sensing of the refractive index when immersed into different solvents.[69] However, the coherent plasmon mode of the embedded arrays was insensitive to changes of the dielectric medium.

A new approach for stabilizing SNP arrays based on immobilizing the particles with a thin layer of poly(methylmethacrylate) (PMMA) was developed in this work. The key advantage of this approach relates to the ability of casting thin PMMA layers in the space between SNPs and not on their surface. This is achievable because PMMA does not wet the silver surface due to poor interaction between the two. The uncoated silver surface remained accessible to the interaction with various molecules and this principle can be potentially utilized in sensing applications of SNP arrays. In addition, this approach allowed addressing a fundamental question about the effect of the dielectric medium on plasmon coupling.

EXPERIMENTAL

MATERIALS

Poly(methylmethacrylate) (PMMA) [MW ~996,000], anisole, 4-aminothiophenol, and poly(4-vinylpyridine) (PVP) were purchased from Sigma Aldrich. Silver (I) oxide and USP Absolute-200 Proof ethanol were acquired from Alfa Aesar and Aaper Alcohol & Chemical Company, respectively. All chemicals were used as received. Microscope glass slides were obtained from VWR. Deionized water with a nominal resistivity of 18 MΩ•cm came from a Millipore Milli-Q water purification system. Ultra High Purity Nitrogen and Ultra High Purity Hydrogen were purchased from Air Gas. PMMA and PVP solutions were made by dissolving a weighed quantity of PMMA or PVP into anisole or ethanol, respectively.

INSTRUMENTATION

UV-visible absorption spectra were recorded using a Shimadzu UV-2501PC spectrophotometer. Electron microscopy images were taken with a Hitachi SEM-4800. Spin-drying was performed using a spin-coater WS-400B-6NPP/LITE (Laurell Technologies Corporation). Topographical images were recorded using an AutoProbe CP AFM equipped with MikroMasch Noncontact silicon cantilevers (NSC11/50) in non-contact mode. The AFM images were processed using MatLAB 2007b. All spectra were processed and figures prepared using Spectra-Solve for Windows (LasTek Pty. Ltd). The Feret's diameter of the particles was calculated using ImageJ for Windows (http://rsbweb.nih.gov/ij/).

SYNTHESIS OF SILVER NANOPARTICLES

Silver nanoparticles were synthesized using the hydrogen reduction method.[15] Briefly, the reaction was carried out in a round bottom flask at 70°C and pressurized to 10 psi with hydrogen gas. The size of the SNPs was controlled by the duration of the reaction. All SNPs used in this study were single crystals with a Feret's diameter of c.a. 120 nm.

FABRICATION OF SNP ARRAYS

Microscope slides were cut into 12 mm x 12 mm sized pieces followed by sonication in water for 30 minutes, drying with a stream of nitrogen gas, and plasma treating for 5 minutes. The cleaned slides were placed into a 0.01% PVP solution and rolled on a hot-dog style roller for a minimum of three hours. After the PVP exposure, ethanol and water rinses were used to remove weakly-adsorbed PVP before placing the slides into an aqueous SNP suspension and rolling overnight. Slides with attached SNPs were rinsed with water followed by ethanol and then dipped into a PMMA solution for 5 minutes. After the exposure to the PMMA solution, the slides were spun-dry at 7000 RPM for 45 seconds.

THEORETICAL MODELING

The quasi-crystalline approximation (QCA) of the statistical theory of multiple scattering of waves (STMSW) was used to model the extinction spectra of partially ordered 2D arrays of SNPs.[70] This is a highly efficient approach for partially-ordered

arrangements of scatterers and was successfully applied previously to metal[71, 72] and dielectric[73] close-packed nanoparticle arrays. According to this approach, the lateral electrodynamic interactions between individual particles in the array were considered as the interference of multiply scattered waves in both the near and far field regions. The resulting field at any point of space was a sum of multiply scattered waves from individual SNPs, including their relative phases. In addition to the incident field, each particle experienced the field produced by all waves multiply scattered by other particles. The spatial distribution of particles in the arrays determines the correlation effects for the electrodynamic interactions and was described statistically by the radial distribution function calculated in the Percus-Yevick approximation for hard spheres.[74]

The extinction spectra of closely-packed 2D array of spherical particles was calculated from the expression:

$$D(\lambda) = -\log\left\{\left|1 - \frac{\pi}{k^2}\sum_l n_0(2l+1)(c_l + d_l)\right|^2\right\} \qquad \text{eq. (1)}$$

where $k = 2\pi/\lambda$ is the wavenumber and n_0 is a surface concentration of SNPs. Instead of n_0 an alternative dimensionless overlapping parameter (η) that determines the fraction of the surface area occupied by particles was employed. The coefficients c_l and d_l that relate to Mie coefficients for individual nanoparticles were calculated from the system of linear equations using the silver optical constants taken from [75] and the radial distribution function [70].

RESULTS AND DISCUSSION

STABILIZATION OF SNP ARRAYS WITH PMMA LAYER

When unstabilized SNP arrays are dried, the particles undergo aggregation due to the surface tension forces associated with drying water (Figure 2.1a). The surface aggregation was an irreversible process and the particles remained aggregated upon re-wetting the arrays. In order to prevent the surface aggregation, the particles were physically immobilized by casting a layer of PMMA between the particles (Figure 2.1b). Note, that chemical attachment of particles does not prevent particles from 'rolling' on the surface and forming aggregates. The thickness of the PMMA layer is governed by the spin-drying speed and the PMMA concentration: the higher the concentration and the slower the spinning speed, the thicker the PMMA layer. The spinning speed was the most critical factor in fabricating consistently uniform layers. All substrates were spun-dried at 7000 RPM because speeds lower than 7000 RPM resulted in non-uniform coverage. Electron microscope images of SNP arrays spun-dried at different speeds revealed that the spinning speed did not affect the interparticle distance (data not shown).

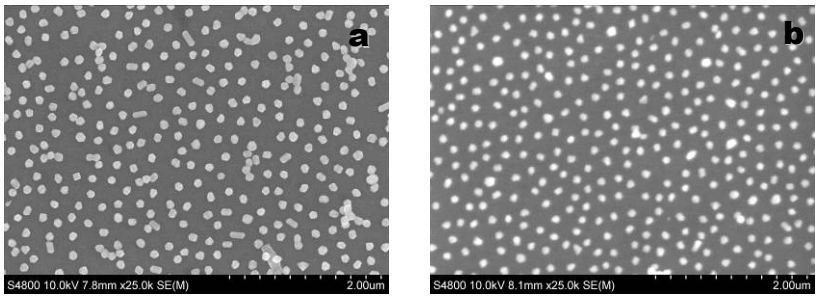

Figure 2.1. SEM images of dried silver nanoparticle arrays (a) without PMMA treatment and (b) treated with 5% PMMA solution.

Atomic Force Microscopy (AFM) was used for measuring the thickness of PMMA between the individual SNPs in the arrays. Figure 2.2 illustrates the effects of changing the concentration of PMMA at the constant spinning speed 7000 RPM. When 0.1% PMMA concentration was used, the layer was too thin to be reliably measured with AFM because its thickness was most likely smaller than the deviation of the particle size (Figure 2.2a); thus, the layer thickness was estimated to be a few nanometers at this concentration. The concentration of 1.0% resulted in a ~15 nm thick layer (Figure 2.2b), 3.0% yielded the thickness of ~90 nm (Figure 2.2c), and 5.0% PMMA completely filled the space between the SNPs (Figure 2.2d).

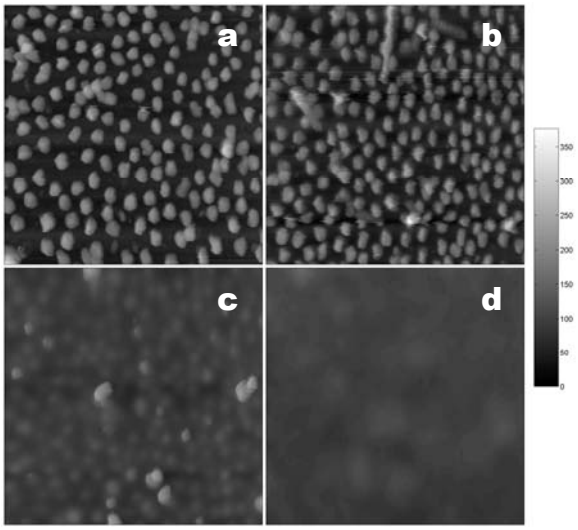

Figure 2.2. AFM images of silver nanoparticle arrays treated with (a) 0.1%, (b) 1%, (c) 3%, and (d) 5% PMMA solutions.

An important question is whether or not PMMA adsorbs to the surface of SNPs and remains there after the spin-drying. Even though PMMA does not contain functional groups that interact with silver, it was still possible that a thin layer of PMMA coated the particles via physiosorption. Such layer could passivate the silver surface preventing its direct accessibility to molecules of interest in potential sensing applications. In order to test the possibility for the interaction between PMMA and silver, the polymer was spun-coated onto plain glass slides that were then immersed into a SNP suspension. The overnight exposure to SNPs did not result in any particles adsorbed to the slides, indicating the lack of the interaction between the two. In a different experiment, SNP arrays spun-dried with 2% PMMA were exposed to a 1.0 mM 4-aminothiophenol solution for 30 minutes and exposed overnight to a SNP suspension. The 4-aminothiophenol molecule contains thiol and amino groups both capable of bonding to silver, and the formation of a second layer of SNPs was expected on the immobilized particles. Indeed, electron microscopy revealed from one to three additional SNPs adsorbed to every immobilized particle in the arrays (data not shown). Based on these experiments, it was concluded that the surface of the silver nanoparticles in the arrays was not covered with a PMMA layer after spin-drying.

THE EFFECT OF THE DIELECTRIC MEDIUM ON PLASMON COUPLING

The coherent plasmon coupling in 2D arrays of SNPs was manifested as a characteristic sharp and intense band in the blue spectral range of the extinction spectrum (Figure 2.3) representing the coherent plasmon mode.[19] The same SNPs in aqueous

suspension exhibit two maxima in the extinction spectra at 502 nm and 415 nm due to the dipole and quadrupole components of the plasmon resonance, respectively. It was experimentally demonstrated by stretching the coupled SNP arrays that the sharp band evolved from the quadrupole component of the plasmon resonance of non-interacting particles.[19] The immobilization of the arrays with PMMA layers provided an opportunity for studying the effect of the dielectric function in the space between the particles on the plasmon coupling.

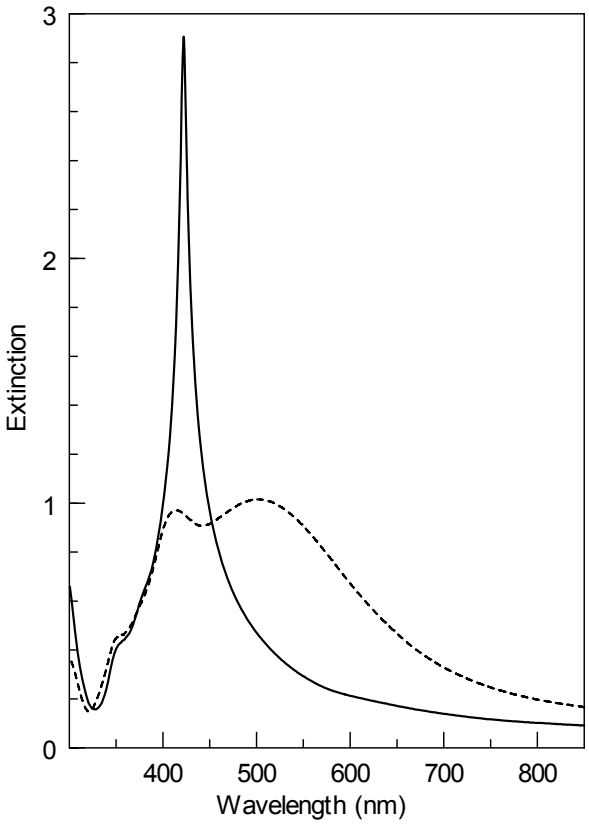

Figure 2.3. Extinction spectra of a strongly coupled 2D array of silver nanoparticles in water (solid) and aqueous suspension of SNPs (dash).

The effect of the local dielectric function on the plasmon resonance of individual particles is well-understood: the resonance shifts to the red spectral region and the polarizability of the particles increases in the media with higher dielectric function.[76-78] This behavior is commonly rationalized in terms of the screening charges induced in the polarizable medium in the close proximity to the particle.[78-80] The charges produce the 'restoring force' to the oscillating electrons, thereby, affecting the frequency and intensity of the plasmon resonance. Higher dielectric function means larger polarizability of the medium and stronger restoring force causing the frequency shift to lower energies. The same argument is applied to plasmon coupling between particles: the dielectric medium shields the local field; therefore, the coupling should be reduced in media with a higher dielectric function.[78-80]

However, the current experiments revealed a different behavior: the strength of the coupling between SNPs in 2D arrays increased in the medium with higher dielectric function. As the PMMA concentration was increased from 0.05% to 5.0%, the effective refractive index in the space between particles increased from that close to 1.0 (air) to c.a.1.49 (PMMA)[81-83], and the arrays became progressively more coupled reaching the maximum coupling when the spaces between the particles were completely filled with PMMA. The maximum coupling was concluded based on the observation of the sharpest and most intense plasmon band in the extinction spectrum of the arrays (Figure 2.4a).

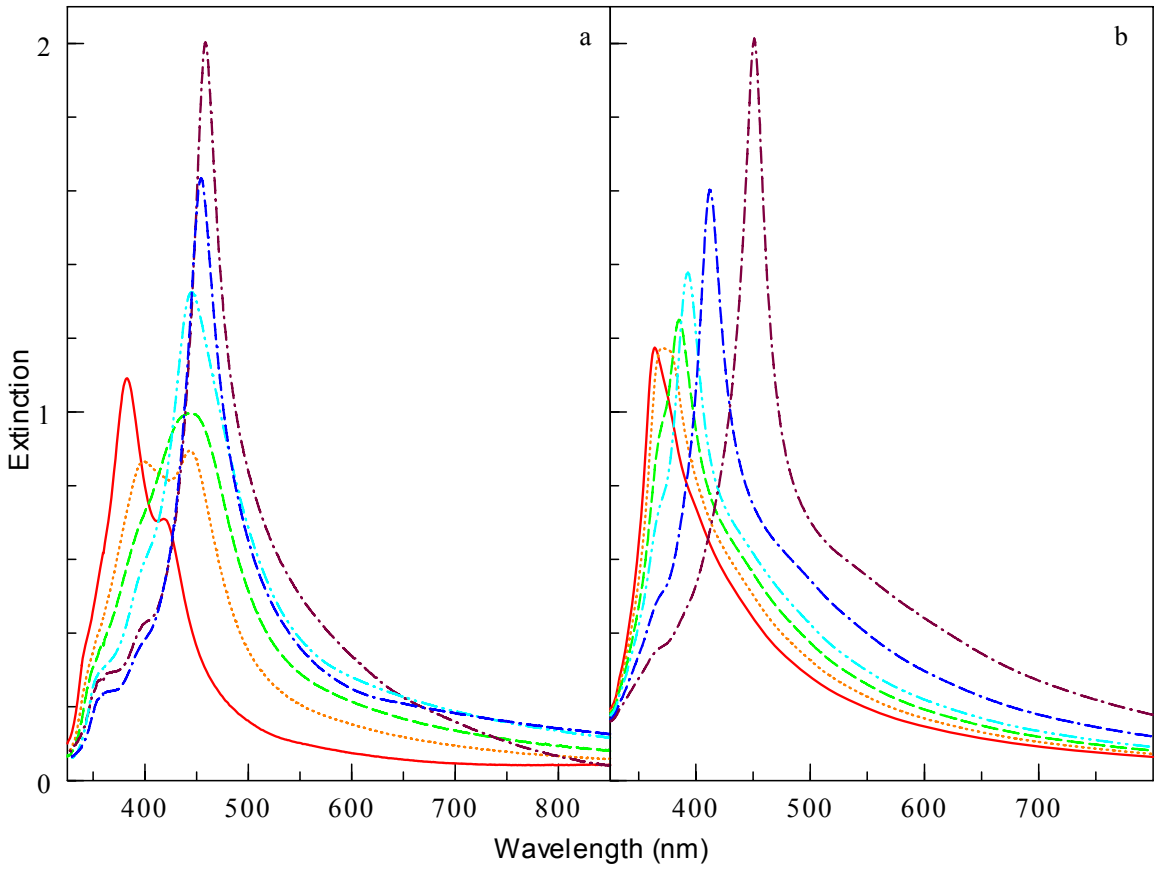

Figure 2.4. Experimental (a) and calculated (b) extinction spectra of silver nanoparticle arrays treated with 0.05% (solid), 0.3% (dot), 0.7% (dash), 1.0% (dot-dot-dash), 3.0% (dot-dash-dash), and 5.0% (dot-dash) PMMA solutions and measured in air.

The intensity of the quadrupole component in the measured spectra exhibited a non-monotonic (having a minimum) dependence on the PMMA thickness (see Figure 2.4a). This behavior can be explained by the combined action of the two competing processes: the increase of the PMMA thickness decreased the free surface of SNPs that leads to reduced intensity of near field waves reflected from the glass substrate and, in this way, results in reduced intensity of the excited quadrupole mode (as we already mentioned above).[84] However, when the interparticle space gets sufficiently filled

with PMMA, plasmon coupling becomes sufficiently strong to turn this dependence: the intensity of quadrupole modes start to increase due to exposure of particles to essentially nonuniform effective field. The experimental spectra agree well with the results of the numerical simulations presented in Figure 2.4b. One can see that increasing PMMA thickness leads to the same effects in extinction spectra as the immersion in water discussed below: surface plasmon band moves to the red spectral region and becomes narrower.

Whereas the spectra in Figure 2.4 were measured in air, the same measurements were also performed with the arrays immersed in water. As expected, water increased coupling for the arrays that were not completely filled with PMMA: the arrays treated with 0.05% PMMA did not exhibit pronounced coupling in air but became strongly coupled in water (Figure 2.5a). On the other end, the arrays that were completely filled with PMMA and already displayed the sharp band did not show any spectral changes upon immersion in water (Figure 2.5d). The intermediate PMMA concentrations produced various degrees of spectral changes from dry to wet states (Figure 2.5b and Figure 2.5c). As the PMMA layer thickness increased, the arrays became less sensitive to the changes of the dielectric function of the surrounding medium.

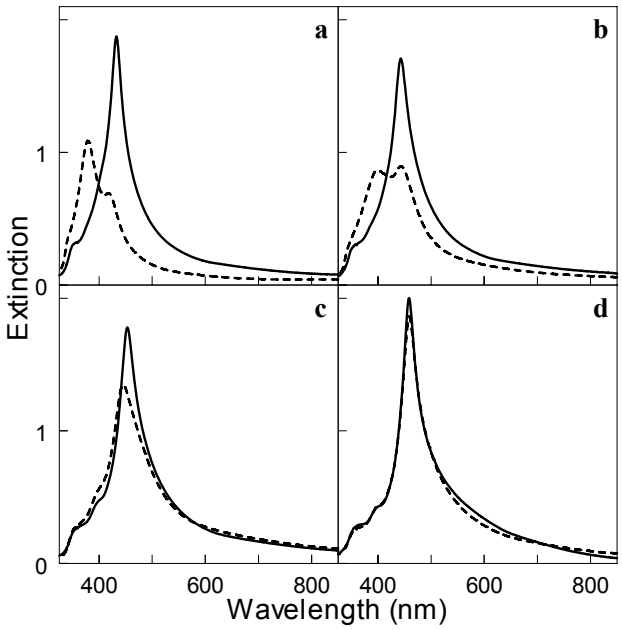

Figure 2.5. Extinction spectra of silver nanoparticle arrays treated with (a) 0.1%, (b) 1.0%, (c) 3.0%, and (d) 5.0 % PMMA solution and measured in air (dash) and water (solid).

It was determined in the previous work that plasmon coupling in 2D arrays of SNPs strongly depends upon the interparticle distance.[19] This dependence provides an opportunity to change the degree of the coupling by changing the particle surface coverage. Non-coupled and weakly coupled arrays were fabricated in this way, in addition to strongly coupled arrays described above, and the effect of the dielectric medium on their optical properties was studied. The particle surface coverage was varied by changing the concentration of SNPs in suspension and/or by varying the exposure time. The films were treated with 0.05% of PMMA and extinction spectra were measured in air and water. Upon immersion in water, the uncoupled films exhibited only red shifts of both quadrupole and dipole components of the plasmon resonance. The extinction spectra of these films resembled that of SNPs in suspension (Figure 2.6a). No

significant coupling was observed in this case because the interparticle distances were too large for the overlap of the local electromagnetic fields from adjacent SNPs. The 20 nm red shift of the dipole component of the arrays in water as compared to the SNPs in suspension was due to the underlying glass substrate. The weakly coupled films exhibited an opposite behavior upon immersion in water: a 16 nm blue shift and sharpening of the plasmon resonance (Figure 2.6b). The blue shift and the sharpening of the resonance relative to those of the SNPs in suspension are indicative of the coherent plasmon coupling. This result further emphasizes the conclusion that increasing the dielectric function of the surrounding medium promotes the plasmon coupling in 2D arrays.

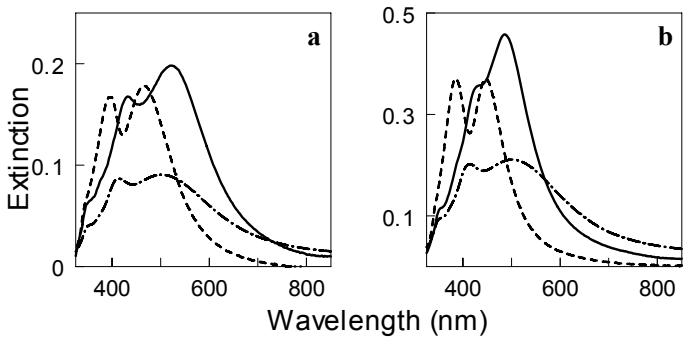

Figure 2.6. Extinction spectra of uncoupled (a) and partially coupled (b) silver nanoparticle arrays treated with 0.05% PMMA solutions and measured in air (dash) and water (solid). Dot-dash line corresponds to the extinction spectrum of silver nanoparticles in aqueous suspension and provided for reference.

The following argument is used to explain this result. Plasmon coupling takes place by means of local fields produced by induced dipole and/or quadrupole moments in closely spaced SNPs. The distance between particles should be smaller than the characteristic length, to which the local field extends from the surface of SNPs, so that each particle experiences local fields from its closest neighbors. Because the local fields from neighboring particles influence each other, the strength of the coupling is proportional to the product of the induced moments from all particles that participate in the coupling. For example, for two identical particles the plasmon coupling will depend on the square of the dipole moment (μ) induced in each particle.[84] The induced dipole moment is expressed as $\mu = \varepsilon_m \alpha \mathbf{E}$, where α and $\mathbf{E}$ are the polarizability and the electric field vector experienced by the particle, respectively, and ε_m is the dielectric function of the surrounding medium.[84, 85] From this equation, the coupling between the two particles is proportional to the square of the dielectric function of the surrounding medium. In the case of the 2D arrays of SNPs, more adjacent particles contribute to the coupling, and a higher power dependence on the dielectric function of the medium is expected. On the other hand, the shielding effect of the medium between SNPs is also increased with larger dielectric function.[78-80] As a result, there are two competing processes as the dielectric function of the medium is increased: one is the increase of the induced dipole moments in the SNPs leading to stronger coupling and the other one is the increase of dielectric shielding that weakens the coupling. The first process, however, makes larger contribution to the coupling because of the higher power dependence on the dielectric function of the medium as compared to the shielding that depends only on the

first power of ε_m.[78] Therefore, the coupling between SNPs in 2D arrays increased and the resonance became sharper in the media with higher dielectric function.

Theoretical modeling also supports stronger coupling in 2D SNP arrays upon increasing the dielectric function of the surrounding medium. The results of the modeling are shown in Figure 2.7 as a map calculated for a range of the refractive index between 1.0 and 2.0. Increasing of the refractive index of the matrix sharpens and red shifts the plasmon peak, and the result commensurates with the experimental data in Figure 2.4a. The modeling results also indicate that there is an optimum refractive index of the matrix that produces the strongest plasmon coupling and the highest quality coherent plasmon mode.

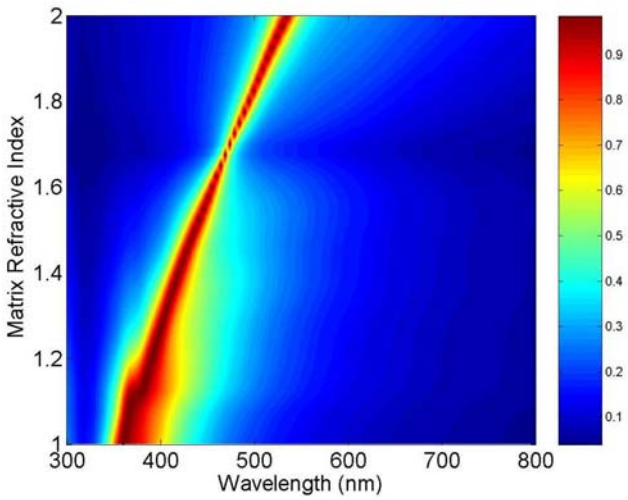

Figure 2.7. Normalized extinction maps of 2D SNP arrays as a function of matrix refractive index and wavelength (η=0.28).

CONCLUSION

The immobilization of SNP arrays with a thin PMMA layer provides a convenient method for stabilizing particles against surface aggregation and preserving their original arrangement. This method provided the opportunity for studying plasmon coupling, specifically how it is affected by the dielectric medium in the space between the particles. Based on experimental data and theoretical modeling, it was concluded that the plasmon coupling is more efficient in the media with higher dielectric function. Employing the quasicrystalline approximation method, the optimum refractive index of the medium was calculated that results in the sharpest coherent plasmon mode with the highest quality factor.

CHAPTER THREE

PLASMON COUPLING IN TWO-DIMENSIONAL ARRAYS OF SILVER NANOPARTICLES: 2 EFFECT OF THE PARTICLE SIZE

INTRODUCTION

The effect of particle size, shape, and surrounding dielectric medium on the optical properties of silver nanoparticles (SNPs) has been investigated for particles in solution.[1] These parameters are not only important for SNPs in suspension, but also in plasmon coupled 2D arrays of SNPs. Even though a great deal of work has been done to investigate the optical properties of plasmon coupled 2D arrays or particles, there are only a few papers that discuss the effect of particle size.

An experimental study by Sung *et. al.* compared two different sized L-shaped and V-shaped particles in 2D arrays prepared by electron beam lithography.[21] A few other research groups have fabricated 2D arrays of triangular and cylindrical shaped particles by either electron beam lithography or nanosphere lithography and investigated the effect of size on plasmon coupling.[23, 25, 86] All of these experimental studies found that as the size of the particles increased in plasmon coupled 2D arrays, the plasmon resonance shifted to longer wavelengths. This result was attributed to the phase retardation effect that occurs when the particle dimensions increase. The effect of particle size on plasmon coupling in dimers[84] and 1D arrays[29] of nanoparticles has also been investigated theoretically, and the plasmon resonance was calculated to shift to longer wavelengths when the particle size is increased.

Presented here is a systematic study of the coherent plasmon coupling in 2D arrays of particles using seven different sizes of silver nanoparticles. It was observed that

the increase of the particle size in coherent plasmon coupled 2D arrays caused the plasmon resonance to shift to longer wavelengths. The size of the particle was also found to be responsible for the intensity of the plasmon coupling. SNPs smaller than c.a. 86 nm did not exhibit intense plasmon coupling as compared to larger particles.

EXPERIMENTAL

Details of experimental procedures were described in the EXPERIMENTAL section of CHAPTER TWO. Briefly, SNPs of different sizes were synthesized by reduction of silver oxide in water with ultra high purity hydrogen gas according to [15]. The 2D arrays were obtained via the self-assembly of SNPs on microscope slides modified with poly(4-vinylpyridine).[87] UV-Vis extinction spectra and electron microscopy images were obtained using a Shimadzu UV-2501PC spectrophotometer and a Hitachi 4800 Scanning Electron Microscope, respectively.

RESULTS AND DISCUSSION

The seven different sizes (c.a. 46, 70, 86, 128, 160, 194, and 287 nm) of silver nanoparticles that were used for the fabrication of 2D arrays are illustrated in Figure 3.1. The electron microscope images are designated (a) through (g) and depict the characteristic shape and dimensions for each of the seven sizes. The corresponding UV-Visible extinction spectrum for each of the SNP suspensions is represented in curves (A) through (G). An important observation in the spectra is that the plasmon bands broaden as the particle size increases. This is due to the phase retardation of the incident radiation

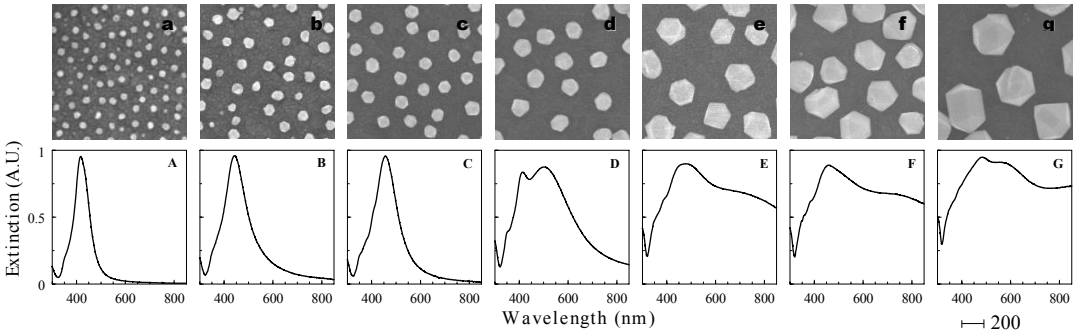

Figure 3.1. Electron microscopy images of c.a. (a) 46 nm, (b) 70 nm, (c) 86 nm, (d) 128 nm, (e) 160 nm, (f) 194 nm, and (g) 287 nm diameter silver nanoparticles. Corresponding UV-Vis extinction spectra of suspensions are designated (A) through (G).

that occurs as the dimensions of SNPs increase.[1, 14] When particles are small as compared to the wavelength of incident radiation, the entire particle experiences the same phase of the incident radiation. As the particle dimensions become larger, the different areas of the particles experience different phases resulting in the formation of multiple plasmon modes. In other words, the particles will respond to more frequencies of the incident light leading to a broader plasmon band. The effect of phase retardation not only plays a role for SNPs in solution but also for particles that are coherently plasmon coupled in 2D arrays.

When SNPs in 2D arrays are brought into close proximity so that their electromagnetic fields overlap with neighboring particles, the system becomes coherently plasmon coupled to yield a sharp plasmon mode.[19] This mode is illustrated in Figure 3.2 for each of the seven different sized SNPs. As the particle size increases, the plasmon coupled peak shifts to the red spectral region, and the corresponding peak positions for curves (a) through (g) are 416 nm, 414 nm, 414 nm, 420 nm, 441 nm, 457 nm, and 493

nm, respectively. This shift is a result of the phase retardation mentioned above. For SNPs that are smaller than c.a. 86 nm, the intensity of the plasmon coupled peak is less intense and broader as compared to that for larger particles. The same observation for small particles in 2D coupled arrays was calculated by Zou *et. al.* for 30 nm particles. Small particles in aqueous suspension only exhibit a dipole mode, so plasmon coupling can only occur through this mode.

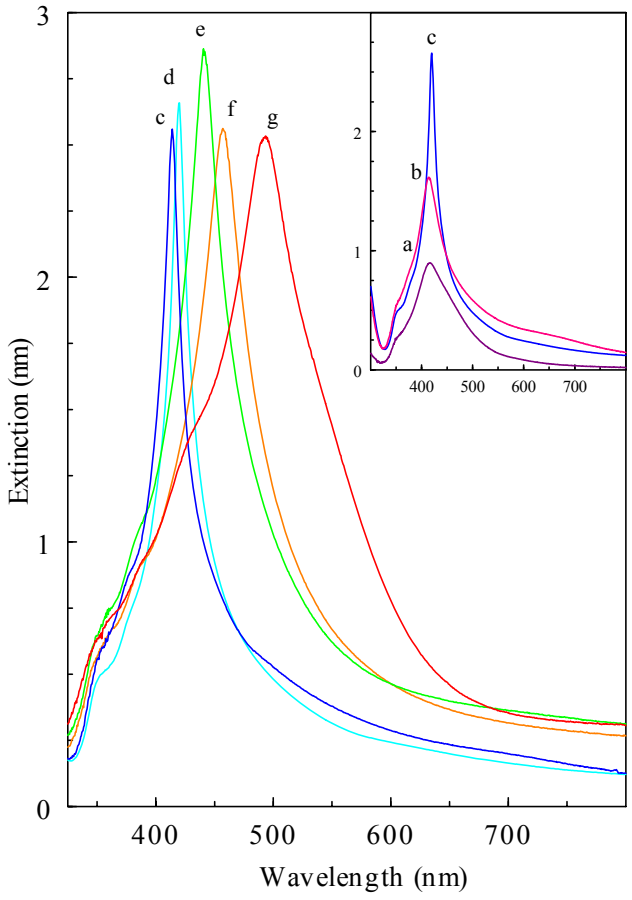

Figure 3.2. UV-spectra of plasmon coupled silver nanoparticle arrays for c.a. (a) 46 nm (b) 70 nm (c) 86 nm, (d) 128 nm, (e) 160 nm, (f) 194 nm, and (g) 287 nm diameter particles.

Once the SNPs become larger, they can couple through higher multipole modes and generate the sharp, narrow plasmon coupled peak. This is illustrated for curves (a) and (b) that are dipole plasmon coupled as compared to curves (c) through (g) which are plasmon coupled through higher multipole modes. Another contributing factor to the red spectral shift is the increase in distance the plasmon resonances must travel inside the particles that results in a lower resonant frequency to maintain a coupled state. This increase in distance translates into longer wavelengths for excitation and, consequently, a red spectrally shifted plasmon peak.

The plasmon coupled peaks broaden as larger particles are used to fabricate the arrays. The broadening is also attributed to the phase retardation of the incident light [1, 30, 88] and has been previously observed.[25] Larger particles interact with more wavelengths of the incident light and result in the excitation of multiple modes in the particles. This translates into more wavelengths for excitation and, consequently, a broader plasmon peak.

Electron microscope images were acquired to illustrate the appearance of the 2D arrays on the glass slides. In order to image the arrays of SNPs on glass slides, the arrays first needed to be immobilized before being dried. Drying of the arrays results in particle aggregation and, therefore, does not give an accurate representation of particle positions.[19] The arrays were immobilized by following a previously reported procedure that used a spin-coater to create a thin layer of PMMA in-between the particles (see EXPERIMENTAL section of CHAPTER TWO). Following immobilization, the arrays were carbon coated to create a conductive layer that is needed

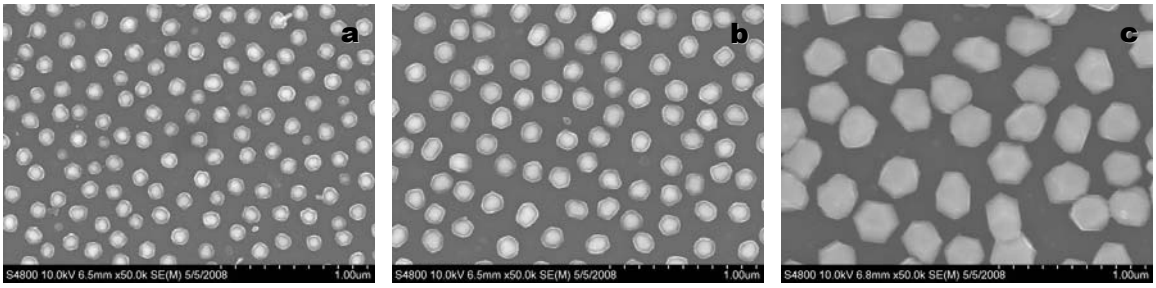

Figure 3.3. Electron microscopy images of silver nanoparticle arrays for c.a. (a) 86 nm, (b) 128 nm, and (c) 287 nm particles.

for electron microscopy. Three different sizes of nanoparticles ((a) 86 nm, (b) 128 nm, and (c) 287 nm) in 2D arrays are illustrated in Figure 3.3. (Note: The halo that appears around the particles is due to the carbon coating and makes the particles appear slightly larger.) These images are representative of the arrays formed on the glass slides.

When the peak position of the coupled plasmon mode is plotted against the size of the particle, a near-linear fit is observed (Figure 3.5) and an R^2 value of 0.95 results. It has also been previously reported that for electron beam lithography and nanosphere lithography produced nanoparticle arrays, the peak position versus the particle size follows a linear trend.[25, 86] This linear trend is very advantageous because now the possibility exists to adjust a lambda maximum by selecting an appropriate particle size. It is important to note that as the particle size increases, there is a larger spread for the potential wavelengths that result. This is illustrated in the spreading of the three points for each size as the particles becomes larger. Even though the particles used in these studies all have an approximate 7% deviation, the spread for the largest particles is 40 nm as compared to 6 nm for the smallest. Additionally, the particle sizes 46 nm and 70 nm

are not included in the plot because the strength of the plasmon coupling is not comparable to larger SNP sizes.

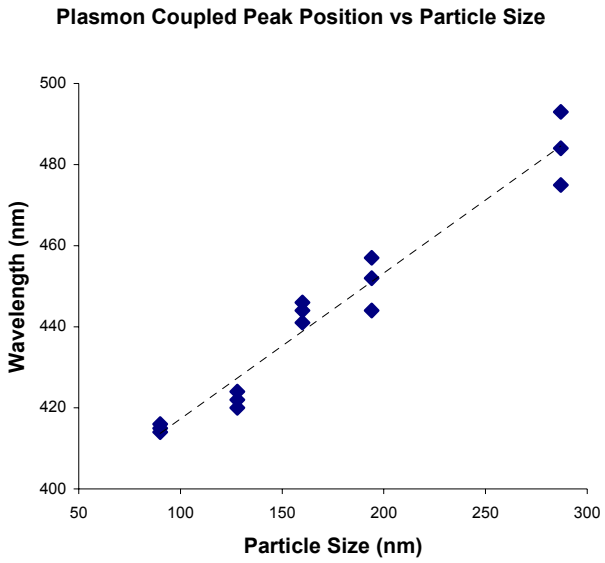

Figure 3.4. Plasmon coupled peak position of coupled plasmon mode plotted against the particle size.

CONCLUSION

The increase in size of the SNPs in plasmon coupled 2D arrays resulted in a red spectral shift of the plasmon peak and is consistent with other literature reports. The spectral shift also followed a linear correlation when plotted against the size of the SNPs. This correlation provides the ability to obtain a specific lambda maximum by selecting the corresponding size. It was also observed that the sharp plasmon coupling only resulted when particles were large enough to experience the excitation of multipole modes.

CHAPTER FOUR

PLASMON COUPLING IN TWO-DIMENSIONAL ARRAYS OF SILVER NANOPARTICLES: 3 EFFECT OF INTERPARTICLE DISTANCE

INTRODUCTION

The optical properties of nanoparticles change with size, shape, and surrounding dielectric medium.[1] These parameters not only apply to nanoparticles in suspension, but also to 2D arrays of nanoparticles. However, another parameter termed interparticle distance also affects the optical properties of 2D arrays. This parameter was investigated for dimers[26, 78, 84, 88-93], chains[24, 25, 94, 95] and 2D arrays[7, 19, 21-23, 25, 29, 30, 96-99] of silver and gold nanoparticles.

It has been found for two interacting nanoparticles (spherical and pyramidal shaped), the plasmon resonance shifted to longer wavelengths as the interparticle spacing decreased.[26, 88, 89] However, when particles were rod shaped the decrease of the interparticle spacing can resulted in either a red or blue spectral shift depending on the polarization of the incident light.[78, 84, 90] For rod shaped particles in a side-by-side orientation, the polarization along the axis of both particles resulted in a large red spectral shift, whereas polarization perpendicular to the axis caused a small blue spectral shift. When unpolarized light was used, the plasmon resonance shifts to the red spectral region because the contribution from the perpendicularly polarized light is minute as compared to parallel polarized. The red spectral shift is caused by the fact that the two particles act like a single larger particle. For chains of nanoparticles, there are fewer examples in the literature but the effect of the interparticle distance on the plasmon resonance was the same as that observed for dimers.

For 2D arrays of nanoparticles, it was observed that the plasmon resonances shifted to shorter wavelengths upon the decrease of the interparticle distance.[7, 21, 29, 30, 97] However, a red spectral shift of the plasmon resonance was observed for 10.5 nm gold nanoparticles in 2D arrays when the interparticle distance was decreased.[96] Another report by Sung *et. al.* showed the plasmon resonance of cylindrical particles resulted in a red spectral shift for 163 nm particles with decreased interparticle spacing, but a blue spectral shift was observed for 339 nm diameter particles.[22]

Here, the effect of the interparticle distance on the coherent plasmon coupling in 2D arrays will be discussed. Depending on the size of the nanoparticles used in the 2D arrays, it was observed that either a blue or red spectral shift of the plasmon peak occurred when the distance between the particles was decreased.

EXPERIMENTAL

Indium Tin Oxide (ITO) coated unpolished Float Glass (Delta Technologies, Limited) with R_s = 4 - 8 Ω were cut into 10 mm x 25 mm slides followed by sonication in hexane for 1 minute and then in water for 15 minutes, drying with a stream of nitrogen gas, and plasma treating for 5 minutes. The cleaned slides were placed into a 0.01% PVP solution and rolled on a hot-dog style roller for a minimum of three hours. Following PVP adsorption to the glass slides, ethanol and water rinses removed any weakly adsorbed PVP from the surface before placing the slides into aqueous suspensions of SNPs containing a know sodium sulfate concentration. The slides were rolled overnight to adsorb SNPs to the PVP layer to create the 2D arrays. After fabrication of the arrays,

the slides were rinsed thoroughly with water to remove any unbound particles and then the UV-Visible spectra of the slides were acquired. The remaining details of the experimental procedures were described in the EXPERIMENTAL section of CHAPTER TWO. In short, silver nanoparticles were synthesized by the hydrogen reduction of silver oxide in water.[15] UV-Visible extinction spectra and electron microscopy images were obtained using a Shimadzu UV-2501PC spectrophotometer and a Hitachi 4800 Scanning Electron Microscope, respectively.

RESULTS AND DISCUSSION

UV-VISIBLE

It was suggested that hydrogen reduced silver nanoparticles have a negative surface charge due to the silver hydroxide on the particle surface.[15, 16] Since the SNPs are in pure water and the surface remains unmodified, they will have a large solvation shell because of the large gradient from the charged particle surface to the low ionic strength of the water. This shell is thick enough to prevent coalescence and gives reason to the high stability and long term (years) storage of hydrogen reduced SNPs. Manipulating the thickness of the solvation shell makes it possible to force the particles closer together. Indeed, the addition of sodium sulfate to a suspension of SNPs resulted in the decrease in thickness of the solvation shell of the particles as will be discussed below. However, too much salt results in the irreversible aggregation of the particles in the suspension. The effect of the solvation shell on plasmon coupling can be observed during the formation of 2D arrays of SNPs.

When an aqueous suspension of SNPs containing no sodium sulfate was used for adsorbing particles to a PVP modified slide, the number of particles on the slide was low and the interparticle distance high. Therefore, the plasmon coupling was weak as illustrated in the red curves in Figure 4.1. As the number of particles on the slide increased, the distance between the particles decreased and the plasmon coupling become more intense (red to orange to green to light blue to blue to violet in Figure 4.1). The dotted green line represents the extinction spectra of SNPs in suspension that were used to make the corresponding 2D arrays.

It was observed for small particles (c.a. 59 nm or less), the plasmon peak red spectrally shifted and broadened as more particles were on the slide. For particles c.a. 86 nm in size, the plasmon peak initially shifted to the blue spectral region as the number of particles on the slide increased, but eventually increased in intensity without shifting. SNPs larger than c.a. 128 nm, resulted in the blue spectral shift and narrowing of the plasmon peak as the interparticle distance decreased. However, there is an optimal interparticle distance for c.a. 128 nm and larger particles because the further increase of the packing density resulted in the broadening and decrease in intensity of the plasmon peak.

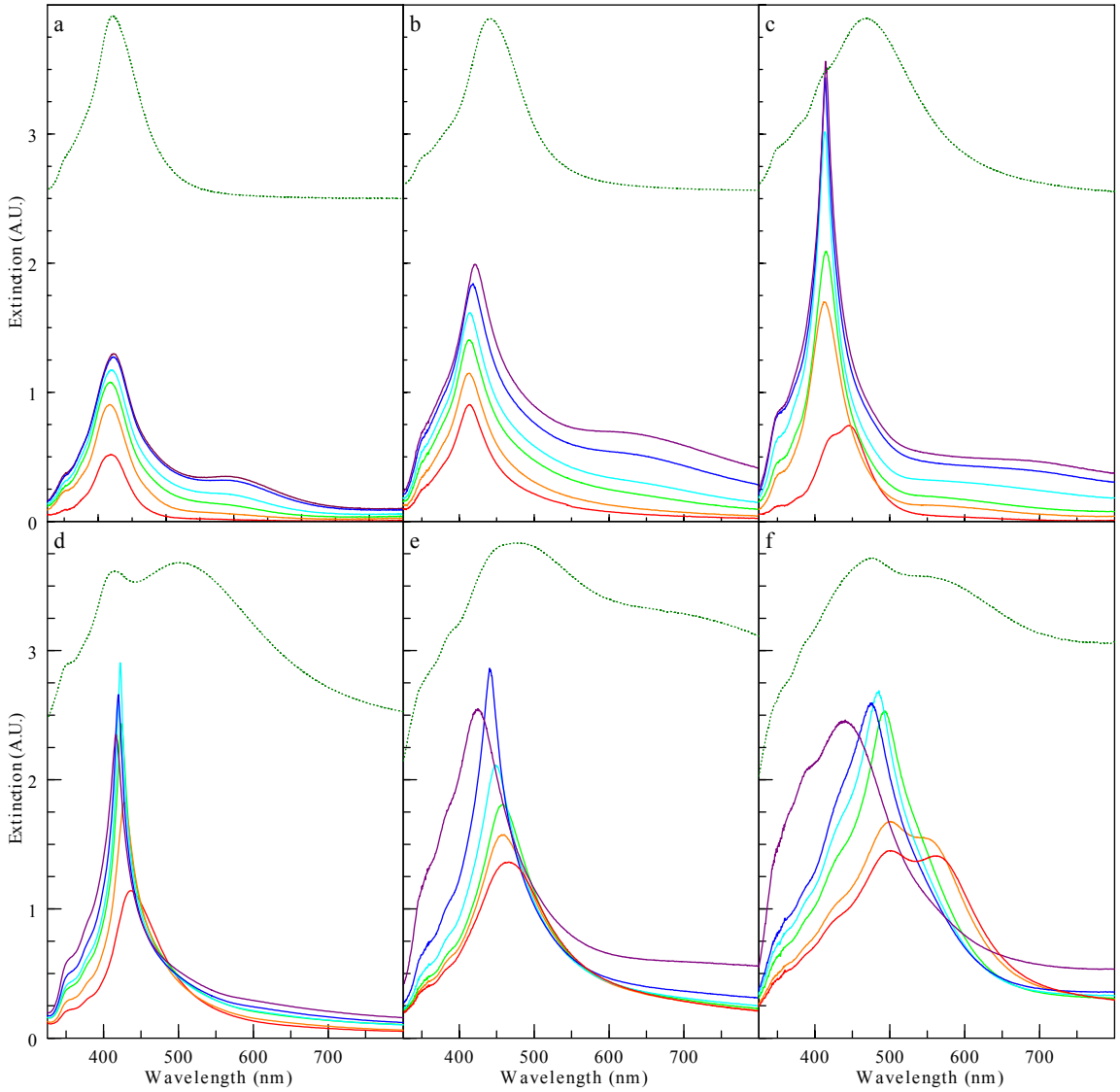

Figure 4.1. UV-Vis spectra illustrating the spectral changes upon increase of the packing density for particles (a) 46 nm, (b) 59 nm, (c) 86 nm, (d) 128 nm, (e) 160 nm, and (f) 287 nm.

In a separate experiment, attempts were made to add more SNPs to a slide that already had adsorbed particles. First, a slide was rolled in a SNP and sodium sulfate solution to adsorb particles to the slide. After adsorption of particles, the slide was rinsed with water, the UV-Visible spectra was acquired, and the slide was placed back into a vial containing a freshly prepared SNP and sodium sulfate solution. It was observed that no new particles adsorbed to the slide because the spectra of the 2D array of particles were identical before and after the second exposure (data not shown). This experiment provided further support that the solvation shell is important and plays a role in the number of particles that can be adsorbed on the slide.

ELECTRON MICROSCOPY

In order to obtain an accurate visual representation of the arrays to compare with their corresponding UV-Visible spectra, the SNPs must be immobilized. This can be accomplished by the spin-casting of a thin layer of PMMA between the particles. For ITO glass slides modified with PVP and exposed to an aqueous suspension of SNPs containing no sodium sulfate, the resulting distances between the particles in the 2D arrays was approximately twice the nanoparticle diameter (Figure 4.2A, 4.2G, and 4.2M.). When slides were exposed to an aqueous suspension of SNPs containing different concentrations of sodium sulfate, the number of adsorbed particles varied. Higher concentrations of sodium sulfate resulted in an increased number of particles in the 2D arrays (Figure 4.2). As the density of particles on the surface increased, the likelihood for aggregation of the particles also increased. This resulted from the PMMA

spin-coating procedure to immobilize the particles. When slides with high packing densities of particles were transferred from water to 2-propanol to anisole, it was believed that the solvation shell became disrupted resulting in the surface aggregation (clumping and stacking) of the particles. This explains Figures 4.2E and 4.2F, for example, which visually appear to have the same packing density.

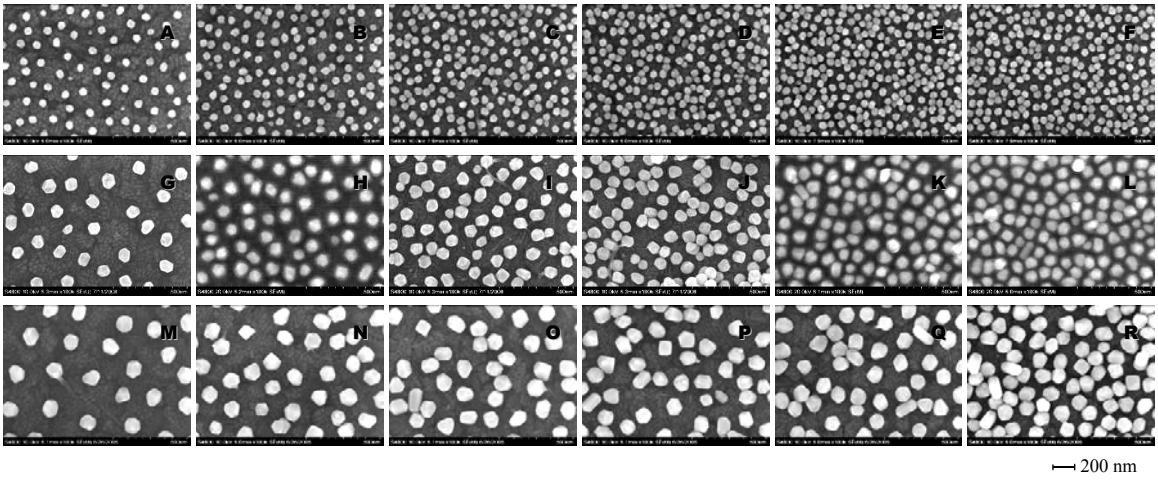

Figure 4.2. The top row (A-F), middle row (G-L), and bottom row (M-R) images are for Figure 4.1b, Figure 4.1c and Figure 4.1d, respectively. The order of the images is left to right for decreasing interparticle distance and correspond to the color of the curves in Figure 4.1b, Figure 4.1c, and Figure 4.1d (red to orange to green to light blue to blue to violet).

Table 4.1 provides quantitative information of the electron microscope images illustrated in Figure 4.2. The column headings are: *Salt* is the concentration of sodium sulfate in the SNP suspension, λ_{max} is the maximum plasmon resonance, *AF* is the area fraction of SNPs on the substrate, *ID meas* is the distance between the center of particles as measured using ImageJ software, and *ID calc* is the calculated interparticle distance. The measured interparticle distances were determined from 100 measurements. Additionally, not all images report an *ID meas* value because the particles are aggregated on the slide and the results would be biased. The calculated interparticle distance was determined by taking a measured area, dividing it by the number of particles in that area, and taking the square root. It is important to note that the concentration of sodium sulfate is dependent on the number of SNPs. For low numbers of particles, a lower concentration of sodium sulfate is needed as compared to higher numbers. To keep all samples consistent, the number of SNPs was kept constant and the concentration of the sodium sulfate was adjusted.

	Figure 4.1b					**Figure 4.1c**					**Figure 4.1d**				
Curve	**Salt (mM)**	**λ_{max} (nm)**	**AF (%)**	**ID meas (nm)**	**ID calc (nm)**	**Salt (mM)**	**λ_{max} (nm)**	**AF (%)**	**ID meas (nm)**	**ID calc (nm)**	**Salt (mM)**	**λ_{max} (nm)**	**AF (%)**	**ID meas (nm)**	**ID calc (nm)**
Red	0.00	417	15.9	134 ± 20	118	0.00	445	14.6	218 ± 34	194	0.00	446	17.6	249 ± 37	208
Orange	1.00	417	29.8	93 ± 14	85	0.50	413	24.5	146 ± 24	134	0.25	436	27.9	203 ± 28	166
Green	3.00	418	39.4	-	77	1.00	415	36.5	129 ± 14	122	0.50	430	32.6	190 ± 24	163
Lt Blue	5.00	419	43.6	-	79	3.00	413	40.4	116 ± 13	106	0.75	427	35.0	-	147
Blue	9.00	422	48.1	-	66	5.00	414	44.0	-	101	1.00	419	37.8	-	146
Violet	15.00	423	49.7	-	66	7.00	415	46.2	-	107	7.00	417	60.1	-	116

Table 4.1. Quantitative data for the electron microscopy images presented in Figure 4.2.

It can be observed from the *AF* values that increasing the concentration of sodium sulfate resulted in an increase in the number of particles on the slides. The λ_{max} values illustrate for 59 nm, 86 nm, and 128 nm particles the plasmon resonance shifts to the red spectral region, does not shift, and shifts to the blue spectral region, respectively, when the interparticle distanced is decreased.

EFFECTS OF INTERPARTICLE DISTANCE

When higher concentrations of sodium sulfate were used, more particles adsorbed to the slide and the risk for particle aggregation on the slide increased. This was observed in Figures 4.1a – 4.1c where the formation of a small, broad plasmon band appears between 550 nm and 800 nm in the spectra. It is important to note that the aggregation observed in the spectra occur before using PMMA to immobilize the arrays. The aggregation of the particles results in the formation of dimers that exhibit a longitudinal plasmon mode in the red spectral region. The longitudinal plasmon mode was an electronic coupling between two particles because the distances are small enough to permit electron tunneling or be touching to form a conductive pathway. The blue and violet curves in Figure 4.1b illustrate the longitudinal plasmon mode, and the averaged surface-to-surface distance between the particles was approximately 7 nm. This value was calculated by subtracting the particle size (59 nm) from the interparticle distance (*ID Calc* = 66 nm).

It can also be observed in Figure 4.1 that the extinction in the spectral region between 600 nm and 800 nm increases in intensity as the interparticle distances are

increased. The behavior of the spectra in this region has resemblance to the spectra of thin silver metal films, and this resemblance could be verified if a tightly packed 2D array of SNPs could be obtained on the slide. Attempts were made to increase the packing density of SNPs on the slide by increasing the sodium sulfate concentration, but higher packing densities (more than what is illustrated in Figure 4.2) of particles could not be achieved. When the SNP and sodium sulfate solution was made, only a limited amount of sodium sulfate can be added before the SNPs coalesce and fall out of solution. The violet curves in Figure 4.1 represent the highest concentration of sodium sulfate that could be used to fabricate the 2D array of SNPs.

The optimum interparticle distance that resulted in the sharpest, narrowest, and most intense coherent plasmon coupling was different for each of the particle sizes. However, the surface-to-surface distance between particles for the optimum interparticle distance in Figures 4.1b-d was near identical. The optimal interparticle distance for c.a. 59 nm, 86 nm, and 128 nm sized particles was 20 nm, 21 nm, and 19 nm, respectively. It has not yet been determined if the 20 ± 1 nm surface-to-surface distance observed is coincidental or represents an optimal distance for the local electromagnetic field to interact with a particle.

In a theoretical study by Zhao *et al.* [100], the effect of interparticle distance on the plasmon coupling of 2D arrays of 30 nm silver spherical particles was investigated. They observed that the intensity of the plasmon coupling decreased and the plasmon band shifted to the blue spectral region as the interparticle distance was decreased. When the interparticle distance reached 75 nm, the plasmon band shifted back to the red spectral

range as the distance continued to be decreased. The 75 nm interparticle distance corresponds to a 45 nm surface-to-surface distance between particles. The results by Zhao *et al.* are different from the experimental data we collected. Even though our particles are 16 nm larger than those used in the theoretical investigation, the sizes could be considered close enough in order to compare their theoretical modeling with our experimental results. We observed an increase in intensity of the plasmon mode upon the decrease of the interparticle distance. In addition, we did not observe the blue spectral shift even though the interparticle distances were comparable to the values reported in the theoretical modeling. Zhao *et al.* have attempted to explain the observations of the red and blue spectral shifts of the plasmon peak for small particles when the interparticle distance is changed by using a theoretical model based on a retarded dipole sum.[100] The blue or red spectral shift results when the real part of the retarded dipole sum is negative or positive, respectively. As previously mentioned, their experimental data and theoretical model do not fit the data presented in this paper. No other discussions regarding 'why' there is a blue spectral shift of the plasmon peak have been reported.

CONCLUSION

The use of sodium sulfate to decrease the thickness of the solvation shell surrounding the SNPs made it possible to increase the packing density of particles on a PVP modified substrate. For particles c.a. 59 nm or less, the decrease of the interparticles spacing resulted in red spectral shifts where as c.a. 128 or larger particles exhibited a blue

spectral shift. It was also found that the sharpest and narrowest plasmon peaks had a surface-to-surface distance of approximately 20 nm.

CHAPTER FIVE

SURFACE ENHANCED RAMAN SCATTERING FROM SILVER NANOPARTICLE ARRAYS ON SILVER MIRROR FILMS: PLASMON-INDUCED ELECTRONIC COUPLING AS THE ENHANCEMENT MECHANISM

INTRODUCTION

Optical properties of silver nanoparticles (SNPs) are determined by the excitation of plasmon resonances – the collective oscillations of the free electron density. Plasmon resonances can be optically excited only in submicron particles but not in the bulk of the metal because of the momentum conservation requirement.[4-8] Optical excitation of plasmon resonances in SNPs constitutes the most efficient interaction of light with matter. By varying the particle size, shape, and surrounding dielectric environment the plasmon resonance can be tuned across the near-UV, visible, and near-infrared spectral range. The high efficiency for interaction with light, tunability of the optical resonance, as well as photochemical robustness makes SNPs attractive for applications in biosensors[8, 9], optical filters[67], plasmonic waveguides[11], and as substrates for surface-enhanced spectroscopies[7, 12, 13].

The excitation of plasmon resonances in SNPs produces an electromagnetic field that is localized around the particles and is enhanced as compared to the incident field. It was experimentally shown that this local electromagnetic field extends 40 nm from the surface of 84 ± 5 nm diameter particles.[17] When several particles are put in close proximity so that the local fields associated with electron oscillations in individual particles overlap, the system becomes plasmon coupled and new plasmon modes result. This plasmon coupling was observed in 2D arrays of SNPs as a sharp band representing a

new plasmon mode in the blue spectral range of the extinction spectra.[19] Plasmon coupling between SNPs and a continuous silver mirror film as well as the effect of this coupling on Surface Enhanced Raman Scattering (SERS) was also studied.[12]

When molecules are on nanostructured silver or gold surfaces they could experience the enhancement of Raman scattering, the phenomenon known as SERS.[34] SERS-active substrates include electrochemically roughened metals [33],suspensions of metal nanoparticles [101] or nanoparticles adsorbed onto surfaces [35], lithographically produced metal nanostructures [38], and vacuum deposited metal island films [36]. Two types of mechanism are currently used to explain the SERS phenomenon: electromagnetic or local field enhancement mechanism (LFEM) due to the enhanced local field from surface plasmons, and chemical enhancement resulting in the increase of molecular polarizability. The role of the enhanced local field is simply to provide increased excitation power to the molecule.[12, 102] LFEM does not require the molecules to be adsorbed on the surface but be confined within the region of the local field near the metal surface.[103]

The chemical mechanism requires a specific interaction between the adsorbed molecule and the metal surface that, in some cases, leads to the formation of a charge-transfer complex. The complex absorbs light at the excitation frequency producing resonance Raman scattering that appears as SERS.[34, 39, 102, 104] The formation of the charge-transfer complex depends on the chemical nature of the adsorbed molecules and the presence of specific sites on the metal surface.[105]

In this work we present experimental results that support a SERS mechanism based on the electronic coupling between adsorbed molecules and the oscillating electrons that constitute the plasmon resonance. This mechanism is different from the charge-transfer mechanism because no visible resonance is observed. Similar interactions between adsorbed molecules and surface plasmons have been previously reported as a source of SERS.[42, 47, 48, 60-62, 106, 107] The studies were performed with a number of molecules adsorbed on silver Nanoparticle Arrays on silver Mirror Films (NAMF) previously developed in this laboratory.[12] The competitive Raman enhancement of different-type molecules that simultaneously interact with the silver surface is described. It is believed that this phenomenon has not been previously reported.

EXPERIMENTAL

MATERIALS

Ag_2O, trans-4-aminocyclohexanol, 4-aminophenol, 4-(2-aminoethyl)aniline, thiophenol, cyclohexylmercaptan, benzyl mercaptan, 2-phenylethanethiol, benzylamine, 2-phenylethylamine, and 3-phenylpropylamine were purchased from Alfa Aesar. Poly(4-vinylpyridine), poly-L-lysine, adenine, methamidophos, 4-mercaptobenzoic acid, 4-mercaptophenylboronic acid, 4-nitroaniline, 4-nitrophenol, 4-aminothiophenol, and 4-phenylbutylamine were purchased from Sigma Aldrich. Hydrogen gas (99.9%) was obtained from National Welder Supply Company. Microscope glass slides were received from VWR. USP Absolute-200 Proof ethanol was purchased from Aaper Alcohol and

Chemical Company. All chemicals were used as received. Water with a nominal resistivity of 18 MΩ•cm was obtained from a Millipore Milli-Q water purification system.

INSTRUMENTATION

The Raman instrument consisted of a spectrograph (Triplemate 1377, Spex) interfaced to a liquid-nitrogen cooled CCD detector (model LN1152, Princeton Instruments,) operating at -120 °C and an Innova 200 argon ion laser excitation source. The SERS spectra were excited with p-polarized light with 514.5 nm wavelength at 1.0-1.1 mW power on the sample. The light was impinging at approximately a 45° angle on the sample, so that both normal and tangential components of the electric vector were simultaneously present. A cylindrical lens was used to focus laser light and produce a 0.1 x 3.0 mm spot on the sample. The total acquisition time for each sample was 100 seconds. The scattered light was collected in a backscattering geometry and analyzed with 1.0 nm spectral resolution. The Raman spectra were calibrated using indene. UV-visible absorption spectra were measured on a Shimadzu UV-2501PC spectrophotometer. All spectra were processed and figures prepared using Spectra-Solve for Windows (LasTek Pty. Ltd).

SYNTHESIS OF SILVER NANOPARTICLES

Silver nanoparticles were synthesized by a hydrogen reduction method previously reported by this laboratory.[15] In short, Ag_2O in water is heated to 70°C in a round bottom flask configuration. The system is purged and pressured with hydrogen to a

pressure of 10 psi. Ag_2O is reduced to silver metal in the form of nanoparticles. The size of the nanoparticles is governed by the duration of the reaction.

FABRICATION OF NAMF SUBSTRATES

Microscope slides were cut into 25 mm x 10 mm slides. The cut slides were rinsed with Millipore water, dried with a stream of nitrogen gas, and plasma-cleaned for 5 minutes. Silver mirror films were deposited by thermal evaporation of the metal at the base pressure 2 x 10^{-6} Torr. 150 nm of silver was deposited onto a 10 nm adhesion layer of titanium. The silver film slides were further modified with either a polymer or other molecules to act as the affixing layer for the silver nanoparticles. The films were exposed to the solution with affixing molecules for a minimum of 4 hours. After extensive washing, the slides were then exposed to a SNP solution with an optical density of 4 and mixed on a hotdog style roller for a minimum of 4 hours.

TIME-DEPENDENT SERS MEASUREMENTS ON NAMF SUBSTRATES

NAMF substrates were placed into a quartz cuvette for SERS measurements and the SERS spectrum was collected before addition of molecules. Without moving the slide or the cuvette, an aliquot of molecules was added to the cuvette and gently mixed for 10 seconds. SERS measurements were performed repeatedly for 10-15 minutes.

RESULTS AND DISCUSSION

UV-VISIBLE REFLECTANCE MEASUREMENTS

NAMF are convenient SERS substrates composed of SNPs immobilized onto silver mirror films (Figure 5.1).[12] The immobilization was originally accomplished via a poly(4-vinylpyridine) layer that strongly binds to the surface of both the silver mirror film and SNPs via the nitrogen atom on the pyridine ring. In this work, poly-L-lysine, 4-(2-aminoethyl)aniline, 4-aminothiophenol, adenine [108], and methamidophos were also used for the affixing layer because they contained two or more functional groups that can bond to silver. These molecules bond to silver surfaces via primary amines, aromatic hydroxyls, nitrogens on purine rings, or nitrogens on pyridine rings. Optical properties of NAMF substrates are determined by the excitation of plasmon resonances in the SNPs as well as the plasmon coupling between the underlying silver mirror film and the nanoparticles. Additional plasmon coupling occurs between individual SNPs that are in close proximity. SERS was measured after exposing NAMF substrates to solutions of different molecules. Typical UV-visible reflectance spectra of NAMF substrates before and after adsorption of the molecules are shown in Figure 5.2. Trace (a) and (b) consist of multiple curves representing different spots on two different PVP NAMF substrates before and after adsorption of mercaptobenzoic acid and adenine, respectively. The nearly identical spectra illustrate the reproducibility and uniformity of different NAMF substrates and the fact that the adsorption of molecules does not significantly alter the arrangement of SNPs.

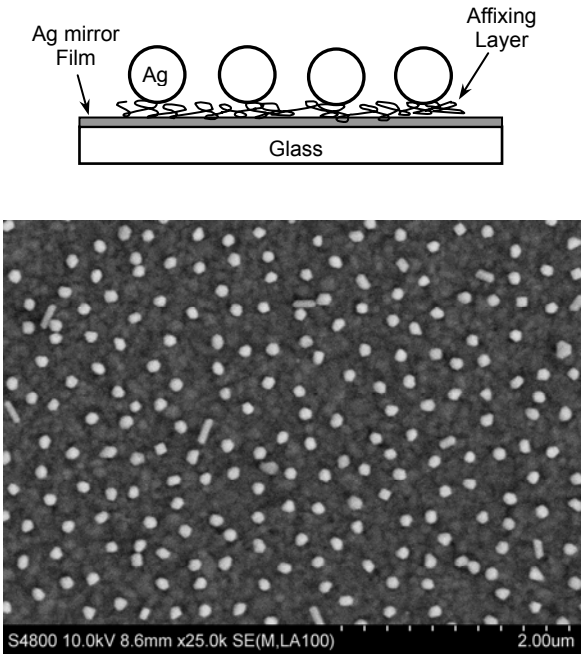

Figure 5.1. Schematic of NAMF substrate (top) and electron micrograph of the substrate (bottom).

Small spectral shifts of the plasmon maxima were observed upon adsorption of the molecules due to the increased local dielectric constant as compared to that of the surrounding solvent. Effort was made to ensure that all reported SERS spectra were measured from NAMF substrates that did not change their UV-visible reflectance spectra upon adsorption of the molecules. In this case, the observed differences in SERS spectra were attributed to the differences in the bond strength of the molecules with the silver surface rather than to changes of the plasmon mode distribution in the NAMF substrates.

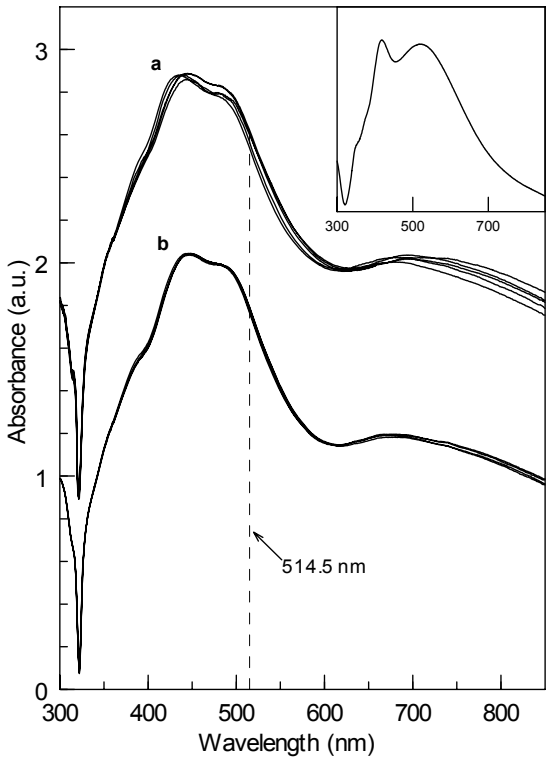

Figure 5.2. UV-visible reflectance spectra of NAMF substrates before and after adsorption of (a) 4-mercaptobenzoic acid and (b) adenine. (Inset) UV-visible spectra of aqueous suspension of silver nanoparticles used for the preparation of NAMF substrates.

SERS

Our goal was to investigate how different chemical structures of molecules affected their SERS. The molecules for these studies were selected based on their ability to bond to silver surfaces (Table 5.1). When used for the affixing layer in the sandwich configuration, compounds 1-6 displayed strong SERS spectra (Figure 5.3). It was expected that the additional exposure of the NAMF substrates to the same molecules would yield more SERS signal; however, no increase of the SERS signal was detected despite more molecules adsorbed on top of the SNPs in the NAMF substrates.

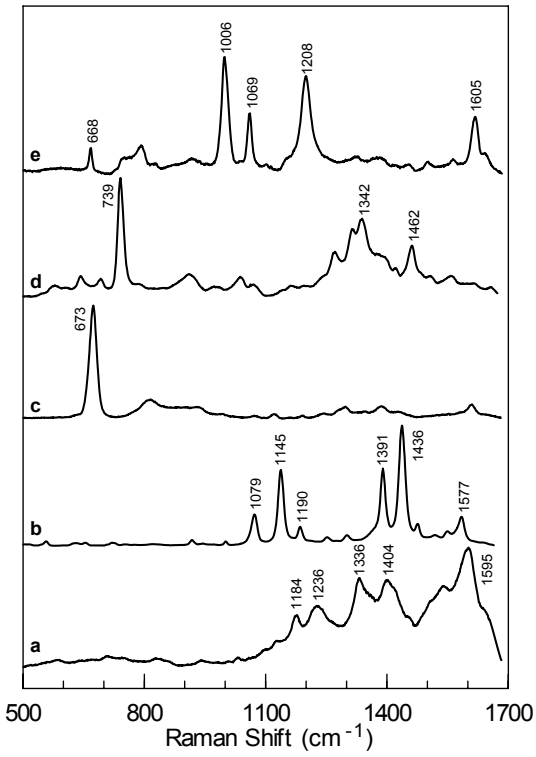

Figure 5.3. SERS spectra of (a) 4-(2-aminoethyl)aniline, (b) 4-aminothiophenol, (c) methamidophos, (d) adenine, and (e) poly(4-vinylpyridine) used as the affixing layer in NAMF.

This adsorption was confirmed in a separate experiment, in which the NAMF substrate with the adsorbed molecules were immersed into a suspension of SNPs and the formation of a second layer of the nanoparticles was observed by the UV-visible reflectance measurement. The lack of an increase of SERS when more molecules were adsorbed suggests that the Raman enhancement mainly resulted from molecules that were in the space between the silver mirror film and the SNPs, and not from the molecules adsorbed on top of and in-between SNPs. If one attempts to explain this result using the LFEM model, the assumption should be made that the NAMF substrate encompasses a distribution of plasmon modes such that the local field was enhanced in the space

between the silver mirror film and the SNPs, and not on top of or in the space between the SNPs themselves. However, experimental evidence indicated the presence of another enhancement mechanism related to the plasmon-induced electronic coupling between the bonded molecules and the silver surface.

No.	chemical name	chemical structure	NAMF	No.	chemical name	chemical structure	NAMF
1	Poly(4-vinyl pyridine)	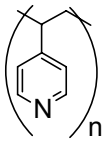	YES	11	Benzylamine	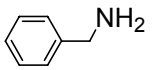	NO
2	Poly Lysine	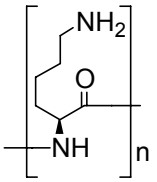	YES	12	2-phenylethyl amine	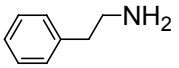	NO
3	Adenine	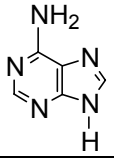	YES	13	3-phenylpropyl amine	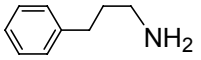	NO
4	methamidophos	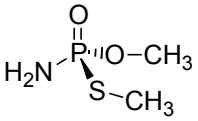	YES	14	4-phenylbutyl amine	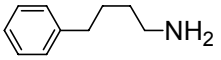	NO
5	4-aminothio phenol	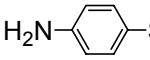	YES	15	4-nitroaniline	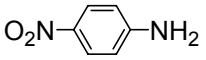	NO
6	4-(2-aminoethyl) aniline	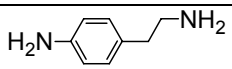	YES	16	4-nitrophenol	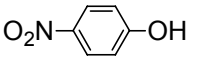	NO
7	thiophenol	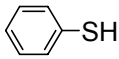	NO	17	4-aminophenol	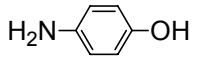	NO
8	cyclohexl mercaptan	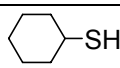	NO	18	trans-4-amino cyclohexanol	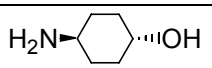	NO
9	benzyl mercaptan	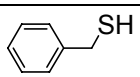	NO	19	4-mercapto benzoic acid	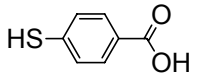	NO
10	2-phenylethane thiol	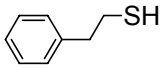	NO	20	4-mercaptophenyl boronic acid	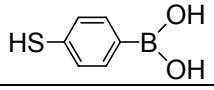	NO

Table 5.1. List of molecules used in this study. NAMF column denotes if a molecule is capable of forming the NAMF structure.

SERS QUENCHING

In these experiments, the SERS signal from molecules in the affixing layer is compared to the SERS signal from dissimilar molecules adsorbed on the NAMF substrate. Based on this comparison, all molecules that were studied can be divided into three categories: (1) molecules that did not yield SERS spectra upon adsorption on the NAMF substrate, whereas SERS spectra from the affixing layer remained visible, (2) molecules that yielded the SERS spectra together with the SERS spectra from the affixing layer, and (3) molecules that yielded strong SERS spectra but completely quenched the SERS spectra from the affixing layer. An observation was made that every molecule from Table 5.1, when adsorbed on the NAMF substrate, partially or completely quenched the SERS signal from the affixing layer. The degree of quenching, which typically ranged from 5% to 100%, was dependent on the strength of the bond of the added molecules as compared to the bond strength of the affixing layer molecules. A typical quenching behavior is shown in Figure 5.4, in which the adsorption of different molecules produced various degrees of quenching of the SERS from the PVP affixing layer. Spectrum (a) corresponds to the PVP affixing layer, and the addition of molecule 4 reduced this spectrum by ca. 30% but produced no additional peaks (spectrum is not shown). The addition of molecule 18 also reduced the PVP SERS spectrum but produced additional weak spectral features assigned to this molecule (curve b). The curves (c-f) in Figure 5.4 illustrate how the addition of molecules 3, 20, 7, and 19, respectively, progressively quenched the PVP SERS spectrum yielding their corresponding SERS spectra.

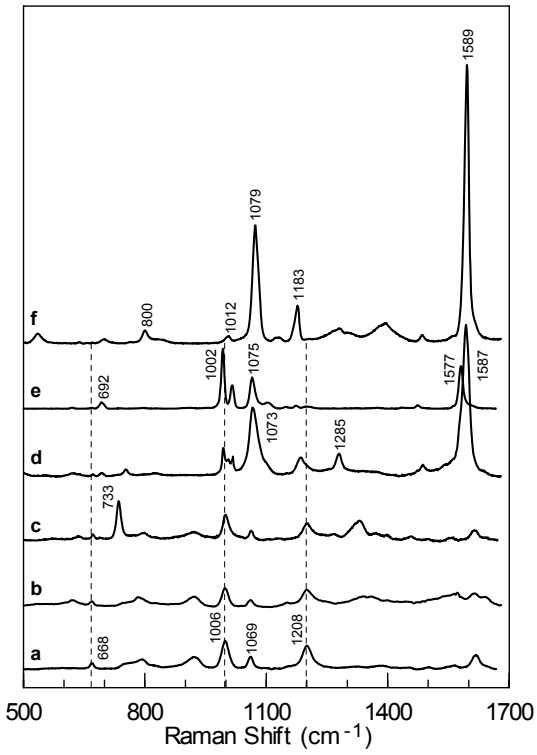

Figure 5.4. SERS spectra of (a) poly(4-vinylpyridine) in the affixing layer and (b) trans-4-aminocyclohexanol, (c) adenine, (d) 4-mercaptophenylboronic acid, (e) thiophenol, and (f) 4-mercaptobenzoic acid added to PVP NAMF substrates.

Other systems that partially quenched the SERS spectra of the affixing layer but did not produce spectra of the adsorbed molecules include molecules 4 and 18 on adenine, 4-(2-aminoethyl)aniline, and 4-aminothiophenol NAMF substrates. A general observation is that all molecules with thiol groups produced strong SERS and completely quenched SERS from molecules in the affixing layer in every NAMF substrate except when 4-aminoethylaniline and 4-aminothiophenol were used for the affixing layer, in which case only partial quenching was observed. These two molecules exhibit a charge-transfer complex when bonded to silver that absorbs light at the excitation wavelength resulting in resonance Raman scattering. The addition of amine-containing molecules

and aromatic hydroxyls resulted in partial quenching of the SERS from all affixing layers. These results can be summarized as the following: the addition of any molecule to any NAMF substrate causes at least partial quenching of the SERS signal from the affixing layer, but may or may not produce a SERS signal itself.

To further illustrate the quenching phenomenon, a time evolution of the SERS signal from PVP and methamidophos NAMF substrates upon the addition of adenine and 4-nitrophenol is shown in Figure 5.5, top and bottom panels, respectively. As time progressed, the SERS intensity from the affixing layer decreased and the SERS intensity of the added molecules increased as more molecules diffused to and adsorbed onto the NAMF substrate. The purpose of these experiments was to verify that there was no interaction between the added molecules and the molecules in the affixing layer. This conclusion was based on the fact that the observed spectra were a simple superposition of the SERS signal from the two species; no spectral shifts of the bands were observed. SERS spectra of all molecules used in these studies were independently measured on aggregated SNPs and were used as a reference when SERS from NAMF substrates was analyzed.

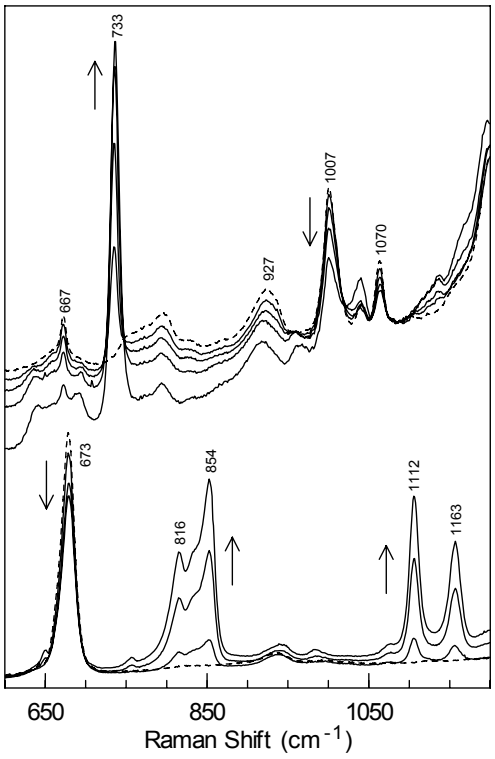

Figure 5.5. Time evolution of the SERS signal from a PVP NAMF substrate upon the addition of adenine (top) and a methamidophos NAMF substrate upon the addition of 4-nitrophenol (bottom).

COMPETITIVE DISPLACEMENT HYPOTHESIS

The most obvious explanation of the observed SERS quenching on NAMF substrates could be competitive displacement of the molecules in the affixing layer by the molecules added to NAMF substrates. This would result in the SERS signal from the affixing layer going down and the SERS of the added molecules going up. A number of arguments and experiments were considered to rule out the competitive displacement hypothesis. Specifically, the 160 kDa PVP polymer is not soluble in water and is unlikely to be displaced by water soluble molecules added to NAMF substrates. If PVP was to be displaced by the added molecules (No. 7-20, Table 5.1) the sandwich structure

would be destroyed because these molecules are not capable of forming the NAMF structure. This was not the case because the NAMF substrates remained intact upon exposure to molecules 7-20 as was evident from the UV-visible reflectance spectra (Figure 5.2). The same behavior was observed for all different combinations of molecules used for the affixing layer and molecules added to NAMF substrates to induce SERS quenching. Any displacement of the affixing layer with another type of molecule is expected to alter the arrangement of SNPs on the mirror film and, consequently, the distribution of the plasmon modes. As was stated above, all SERS measurements were made from NAMF substrates that did not change their UV-vis reflectance spectra upon the addition of any of the molecules listed in Table 5.1.

Other experiments were conducted to determine whether the added molecules quenched the SERS from the affixing layer by intercalating between this layer and the SNPs. In other words, the NAMF substrate structure would change from [silver mirror film - affixing layer – SNPs] to [silver mirror film - affixing layer - layer of added molecules – SNPs]. PVP-modified silver mirror films were exposed overnight to adenine, 4-nitrophenol, 4-aminophenol, trans-4-aminocyclohexanol, and 4-mercaptobenzoic acid followed by the immersion into a suspension of SNPs. In the case of 4-nitrophenol, 4-aminophenol, and 4-mercaptobenzoic acid no immobilization of the nanoparticles on the substrate was observed. It is difficult to conclude whether the molecules displaced PVP from the mirror film or the molecules adsorbed on the PVP layer and caused its ‘passivation’ preventing the adsorption of SNPs. In the case of adenine and trans-4-aminocyclohexanol added to the PVP modified silver mirror films,

SNPs were immobilized; however, the particle density was substantially lower compared to when PVP and adenine were used alone. SERS behavior of these low-density NAMF substrates was different: the addition of adenine resulted in the SERS spectrum of adenine with no visible peaks of PVP, whereas the exposure to trans-4-aminocyclohexanol resulted in the SERS spectrum of only the PVP affixing layer. The formation of low-density NAMF substrates upon the addition of adenine and trans-4-aminocyclohexanol indicates that both molecules adsorb on and partially passivate the PVP layer so that less SNPs immobilize on silver mirror films. This behavior was somewhat surprising because, in the case of adenine, both adenine and PVP are capable of forming high-density NAMF structures, and one would expect that their mixture also results in high-density adsorption of SNPs. To explain this discrepancy one should assume that most of the adenine molecules were bound to PVP in a configuration so that the two species lost their ability to bind SNPs. However, a small fraction of adenine molecules retained their binding properties to nanoparticles forming low-density NAMF substrates and producing weak SERS. Trans-4-aminocyclohexanol, on the other hand, cannot alone form NAMF substrate, and the formation of low-density NAMF substrates upon its addition to PVP-modified silver mirror films was most likely due to the adsorption of SNPs to the PVP layer that was not completely passivated by trans-4-aminocyclohexanol. The observation of only PVP SERS spectrum supports this interpretation. Therefore, it was concluded that adenine and trans-4-aminocyclohexanol did not displace the PVP layer from the silver mirror films, otherwise, a high-density NAMF substrate would form in the case of adenine and no NAMF substrate would form

after the addition of trans-4-aminocyclohexanol. These experiments also indicate that the molecules did not intercalate between the affixing layer and SNPs when SERS quenching was observed, otherwise large alterations of UV-visible reflectance spectra due to changes in SNP packing would be expected.

The experimental results indicate that the observed SERS quenching cannot be explained via the competitive displacement of the molecules in the affixing layer by the molecules added to NAMF substrates. Also, the addition of the molecules did not change the distribution of plasmon modes in NAMF substrates, thereby ruling out the possibility that the observed SERS changes related to the LFEM. A logical conclusion is that the quenching reflects the competitive enhancement of the Raman scattering from different types of molecules simultaneously present on NAMF substrates. This competitive enhancement is sensitive to the chemical nature of the molecules and appears to correlate with the binding strength between adsorbed molecules and the silver surfaces. For example, when PVP was used as the affixing layer, aromatic thiols produced strong SERS and completely quenched the PVP signal whereas all other molecules resulted in various degrees of quenching and SERS intensities. Aromatic amines caused partial quenching and yielded weaker SERS whereas nonaromatic amines produced weak quenching without SERS. Nonaromatic thiols yielded weak SERS but did not produce complete quenching.

In most quenching experiments, high concentrations of molecules in the 10^{-4} – 10^{-3} M range were added to NAMF substrates to ensure saturation of the silver surface with the molecules during a 10 min exposure. Furthermore, high concentrations of

molecules should increase the competitive displacement if such existed. Longer exposure times and higher concentrations did not increase the SERS signal from the molecules or the degree of quenching of the SERS signal from the affixing layer. Lower concentrations (down to 10^{-6} M) required longer exposure times to reach equilibrium but produced the same competitive enhancement as seen with higher concentrations. This independence of the concentration and exposure time further supports the competitive Raman enhancement as opposed to competitive displacement of the molecules in the affixing layer.

SERS RECOVERY

It was understood that the best supporting evidence to exclude the competitive displacement hypothesis for the SERS quenching phenomenon can be obtained if the SERS signal from the affixing layer can be recovered after it was quenched. The main challenge with recovery experiments related to the displacement of molecules originally added to induce quenching with other species that cause quenching to a lesser degree. As previously stated, the degree of quenching appeared to correlate with the relative strength of binding to the silver surface of the molecules in the affixing layer and added molecules. This implies that, in order to displace the quenching molecules, species with stronger affinity to silver must be added; however, these species will most likely induce even more quenching. Indeed, many combinations of different affixing layer, SERS quenching, and displacing molecules were tried but did not produce the recovery effect. More quenching of the SERS signal from the affixing layer was observed upon the

addition of these species. When methamidophos was used as the affixing layer, the addition of 4-nitroaniline caused a small (5 ± 1 %) and reproducible quenching of SERS of methamidophos. 4-nitroaniline weakly binds to silver and can be easily desorbed from the NAMF substrate by rinsing with water. The rinsing resulted in complete recovery of the SERS of methamidophos. In a modified approach, 2-phenylethanethiol was used at low concentration for a short exposure so that only partial quenching of the SERS from the PVP affixing layer was obtained. Next, 10^{-6} M of adenine was added to the system causing small quenching of SERS from 2-phenylethane thiol as well as additional quenching of SERS from the PVP affixing layer. Lastly, 10^{-6} M of potassium iodide was added to the solution with the NAMF substrate and 10 ± 2 % recovery of SERS from 2-phenylethane thiol was observed while SERS from adenine decreased.

The two experiments demonstrate that the molecules were not displaced from the silver surface and the observed SERS quenching is due to the competitive Raman enhancement from different types of molecules simultaneously present on NAMF substrates. The competitive enhancement means that the Raman spectrum of added molecules underwent enhancement at the expense of the Raman enhancement of molecules that were already present in the system. This process depends on the specific chemical interaction between molecules and silver surface, so that the stronger the interaction, the more intense is the SERS signal and SERS quenching. This interaction results in the short-range enhancement of Raman scattering from the molecules that extends to the distance of the electronic coupling between the molecules and the silver surface. The distance dependence of the enhancement was addressed in a series of

experiments in which SERS of the aromatic ring was monitored as a function of the length of the hydrocarbon chain that separated the aromatic moiety from the silver surface. The spectra were also compared to normal Raman spectra of the same molecules in solution.

COMPARISON OF SERS WITH NORMAL RAMAN

Normal Raman spectra of thiophenol, benzyl mercaptan, and 2-phenylethane thiol were measured from neat solutions and normalized to their concentrations so that the band intensities represent relative molecular polarizabilities (Figure 5.6a). The frequency of the symmetric (c.a. 1000 cm^{-1}) and asymmetric (c.a. 1024 cm^{-1}) breathing modes as well as the C-C stretch in the ring (1584 cm^{-1}) increased as CH_2 groups were added between the thiol and the aromatic ring. These shifts are due to the screening of the thiol group from the ring by the addition of CH_2 groups. Another prominent band in the spectrum of thiophenol is at 1092 cm^{-1} corresponding to the C-S stretch at the aromatic carbon. Importantly, the intensity of the symmetric breathing mode decreased only slightly for molecules with zero, one, and two CH_2 groups with the intensities scaling down as 1.0 : 0.68 : 0.59, respectively, as determined for the 1000 cm^{-1} band. The effect is most likely due to the increase of the effective mass of the substituting chain on the aromatic ring. Additionally, the ratio of the C-C stretch and the symmetric breathing mode in the ring for all three molecules remained constant around 0.18.

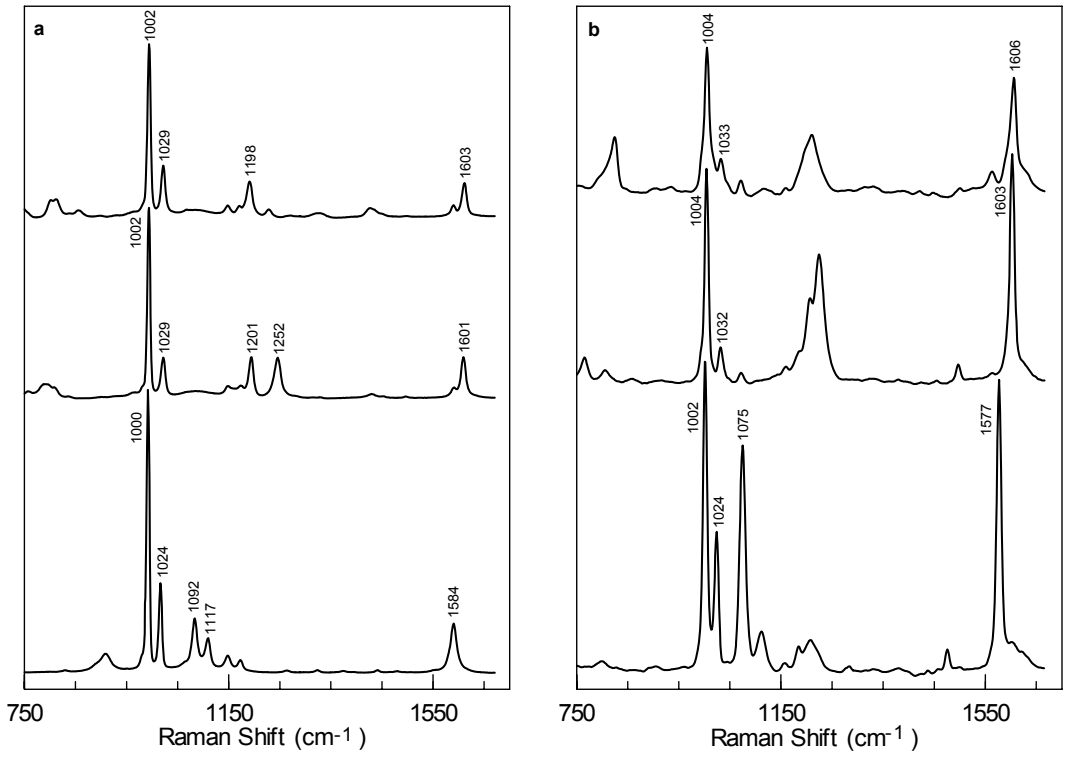

Figure 5.6. Raman (a) and SERS (b) spectra of thiophenol (bottom), benzyl mercaptan (middle), and 2-phenylethanethiol (top).

SERS spectra of the same molecules adsorbed on NAMF with PVP as the affixing layer are different from the normal Raman with respect to both the band frequencies and band relative intensities (Figure 5.6b). Also, new bands appeared in the SERS spectra. The frequency shifts resulted from small changes in the structure of the molecules caused by the adsorption to the surface whereas changes of relative band intensities in the same molecule reflect changes of the transition polarizability tensor due to alterations of the electronic configuration and/or molecular structure. The two prominent differences between SERS and normal Raman spectra are the increase of the intensity of the C-C stretch relative to the symmetric breathing mode for the same molecules and the decrease

of the overall SERS intensity between different molecules with zero, one and two CH_2 groups. Also, the C-S mode at 1075 cm^{-1} is shifted and strongly enhanced as compared to the normal Raman spectrum. Whereas the ratio of the C-C stretch to the symmetric breathing mode was 0.18 in the normal Raman spectra, this ratio increased to 0.8 ± 0.1 for all three molecules in the SERS spectra. Between the three different molecules, normal Raman spectra scaled down as 1.0 : 0.68 : 0.59 and the SERS spectra scaled down as 1.0 : 0.61 : 0.32. By accounting for higher packing density on silver of molecules 9, and 10 as compared to molecule 7,[34,35] the actual decrease of the SERS intensity per molecule for one and two CH_2 groups is even greater as compared to the molecule with zero CH_2 groups. The same trend was also observed for molecules 11-14 in which an amine group in place of the thiol group is separated by one, two, three, and four CH_2 groups, respectively (Figure 5.7). The discussion of these spectra is omitted for brevity. The decrease of the SERS intensity with the distance from the silver surface was attributed to the SERS mechanism and not to the differences in molecular polarizabilities.

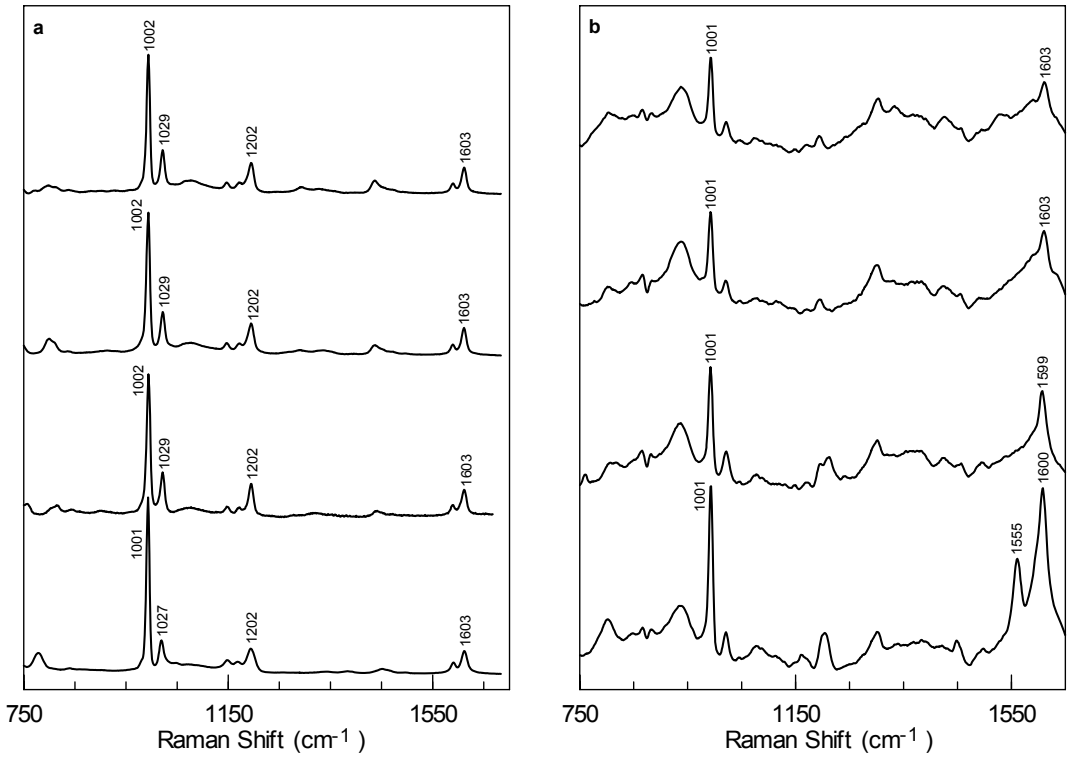

Figure 5.7. Raman (a) and SERS (b) spectra of benzylamine, (bottom) 2-phenylethylamine (second from bottom), 3-phenylpropylamine (second from top), and 4-phenylbutylamine (top).

SERS MECHANISM

The competitive Raman enhancement, the observed differences between normal Raman and SERS spectra, and the distance dependence of the enhancement cannot be explained within the frame of either LFEM or charge-transfer models. According to the LFEM model, for example, the addition of molecules to the PVP NAMF substrate should not quench SERS of PVP but produce a SERS signal characteristic of both species. The same model should yield similar normal Raman and SERS spectra and follow the same intensity pattern when the aromatic ring is separated from the silver surface by CH_2 groups. With respect to the charge-transfer model, it is unlikely that molecules 1-20

interacting with silver through different chemical moieties would all exhibit a ground-state charge-transfer complex in resonance with the excitation wavelength; however, evidence of the formation of such a complex was previously reported for 4-aminothiophenol.[45]

Here, we propose a different mechanism for SERS that is based on plasmon-induced electronic coupling. This mechanism combines the excitation of plasmon resonances in metal nanostructures and a specific chemical interaction of molecules with the metal surface. This interaction is not required to lead to a resonant charge-transfer complex between the molecules and the surface, but it should provide the coupling between the electronic system of the adsorbed molecules and the electron density in the metal. When molecules bind to the metal surface, a conductive pathway is created for the free electrons from the metal to couple with the electronic system of the adsorbed molecules. The type and strength of the bond determines the efficiency of this coupling. The presence of so called 'active sites', such as adatoms, crystal defects, and crystal boundaries on the surface of the metal facilitates the binding and electronic coupling.[109] Upon the excitation of the plasmon resonances, the oscillating electrons in the metal penetrate into the electronic system of the adsorbed molecules causing molecular polarization. This process constitutes the plasmon-induced electronic coupling between the molecules and the metal. The oscillating electrons that comprise the plasmon resonance become a part of the electronic system of the adsorbed molecules. In other words, the plasmon resonance 'extends' into the adsorbed molecules causing the enhancement of their Raman scattering. The following is a summary of the proposed

mechanism based on the plasmon-induced electronic coupling: (1) the molecules adsorbed on the NAMF substrates form a bond with the metal; (2) incident light excites electron oscillations (plasmon resonances) in the NAMF substrates; (3) the bond between molecules and the metal provides the pathway for the oscillating electrons from the metal to penetrate into the molecules (plasmon-induced electronic coupling); (4) different molecules form bonds that provide different degrees of plasmon-induced electronic coupling; (5) when the oscillating electrons penetrate into molecules they induce strong molecular polarization; (6) this strong molecular polarization results in enhanced Raman scattering in which light is scattered by the combined system comprised of the NAMF substrate and the adsorbed molecules. Raman scattering is enhanced because the excitation of plasmon resonances in NAMF substrates causes the oscillating electrons from the metal to penetrate into the electronic system of adsorbed molecules inducing strong molecular polarization. It is important to emphasize that the excitation of plasmons in NAMF is a resonant process, whereas the penetration of the oscillating electrons into the adsorbed molecules is a nonresonant process. This is similar to the normal Raman scattering process where the incident light polarizes molecules in a nonresonant way. In the proposed model, the adsorbed molecules are polarized by the penetrating electrons from the metal and not by the incident light. To be more precise, the polarization of molecules via the penetrating electrons is more efficient than the polarization of the molecules via the direct interaction with the incident light.

A graphical illustration of this process is depicted in Figure 5.8, in which (a) and (b) correspond to the electron oscillations in the absence and presence, respectively, of

the adsorbed molecules. In the absence of the molecules, resonantly scattered light with unchanged frequency (resonance Rayleigh scattering) is the main component, whereas the addition of molecules results in the appearance of Raman-shifted components. Note that the Rayleigh and Raman scattering are both produced by the oscillating electrons in the metal because these electrons exhibit much higher polarizability under irradiation as compared to the molecule itself. The oscillating electrons are modulated with the vibrational frequencies of adsorbed molecules via the process of the plasmon-induced electronic coupling, as described above. A different variation of this mechanism is depicted in Figure 5.8c, and is believed to occur in NAMF substrates for molecules in the affixing layer. In this case, plasmon-induced electronic coupling extends through the molecules and into the silver mirror film, and the Raman enhancement from the molecules in the affixing layer is expected to be even larger. Indeed, molecules 1-6 produced several times stronger SERS when used for the affixing layer as compared to the same molecules adsorbed on top of the particles in NAMF substrates. A related SERS mechanism was previously described in which Raman enhancement originated from the oscillating electrons that tunnel through the molecules adsorbed in the junction between two plasmonic nanoparticles.[39]

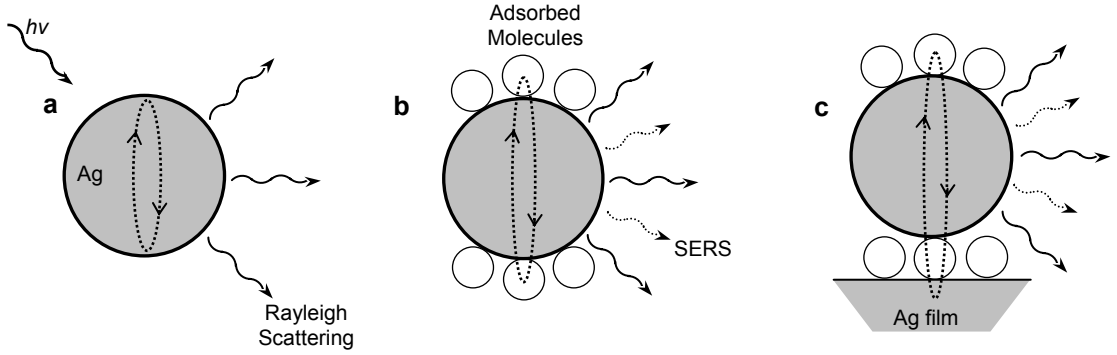

Figure 5.8. Graphical illustration of the electron oscillations in SNPs without adsorbed molecules (a), the plasmon-induced electronic coupling SERS model of molecules adsorbed on an individual SNP (b), and the plasmon-induced electronic coupling SERS model of molecules on NAMF (c).

The observed SERS behavior of different molecules on NAMF substrates can be explained using the proposed plasmon-induced electronic coupling model. According to this model, the competitive Raman enhancement is due to the competitive coupling of the oscillating electrons with different molecules that are simultaneously bound to the silver surface. The oscillating electrons follow the pathway of least resistance; the molecules that provide the pathway of least resistance undergo the strongest SERS at the expense of other molecules that are weakly coupled. The changes in relative intensities of the Raman and SERS bands as well as the appearance of new bands in SERS spectra reflect different origins of the molecular polarization: the polarization via the plasmon-induced electronic coupling in the case of SERS and polarization by the electromagnetic field in the case of normal Raman scattering. Because the two polarizations have different origins, they are characterized by different transition polarizability tensors resulting in different Raman intensities (SERS versus normal Raman) from the same molecule. The

observed decrease of the SERS intensity from the aromatic ring with the addition of CH_2 spacer groups (Figure 5.6b and Figure 5.7b) is due to the diminishing plasmon-induced electronic coupling with the ring. The SERS mechanism based on plasmon-induced electronic coupling does not exclude the presence of other mechanisms on the NAMF substrate, specifically LFEM. The adsorbed molecules could experience the enhanced local electromagnetic field that is concentrated by plasmon resonances; however, LFEM does not appear to be the major contributor to the overall SERS signal.

As mentioned in the SERS QUENCHING section above, the competitive Raman enhancement is dependant on the strength of the bond between the molecules and silver surface. The data presented in Figure 5.4 can be explained using hard-soft-acid-base (HSAB) theory which states that hard acids bind to hard bases and that soft acids bind to soft bases.[110] Silver is a soft acid and binds strongly to the soft base R-SH but has a weaker interaction with the borderline acid/base species pyridine. An amine group, on the other hand, is a hard base and results in a weaker bond with silver. When, for example, a thiol group and a pyridal group are simultaneously bonded to a silver nanoparticle, the stronger bond with the thiol group creates the more efficient pathway for the oscillating free electron density in the silver to penetrate into the bonded molecules. Therefore, hard and borderline base species bonded to silver will result in a less efficient pathway and generate weaker (or no) SERS. This explains why molecules such as 4-mercaptobenzoic acid or thiophenol completely quenched the signal from the PVP affixing layer. Based on the correlation between the HSAB theory and the degree of quenching of the PVP affixing layer, the possibility exists to predict the SERS behavior

of molecules bonded to silver. Research is currently being done in our laboratory to further investigate the relationship between SERS and HSAB theory.

CONCLUSION

Based on the analysis of SERS spectra from twenty different molecules, plasmon-induced electronic coupling between the adsorbed molecules and the silver surface was concluded to be the major contributor to the SERS on silver nanoparticle arrays on silver mirror films. It is believed that this mechanism has general applicability to other systems that exhibit SERS. Two main requirements should be fulfilled to observe strong SERS: the system should have plasmon resonances at the wavelength of the excitation and the molecules should bind to the metal surface via chemical interaction that provides electronic coupling. The degree of quenching that was observed for the affixing layer was proportional to the strength of the bond between the added molecules and silver surface. Molecules with thiol groups bond strongly to silver and completely quenched SERS from the affixing layer. Bonds between amine groups with silver are weaker and, therefore, only resulted in partial quenching of the affixing layer SERS. In addition, molecules with the conjugated electronic structure exhibit stronger SERS due to both large intrinsic polarizabilities and better coupling with the electron density in the metal.

CHAPTER SIX

PLASMA REDUCTION OF SILVER COMPOUNDS FOR FABRICATION OF SURFACE ENHANCED RAMAN SCATTERING SUBSTRATES

INTRODUCTION

Molecules near nanostructured silver or gold surfaces could experience the enhancement of Raman scattering, the phenomenon known as Surface Enhanced Raman Scattering (SERS).[34] Traditional SERS-active substrates include electrochemically roughened metal surfaces [33], suspensions of metal nanoparticles [101] or nanoparticles adsorbed onto surfaces [35], vacuum deposited metal island films [36], and lithographically produced metal nanostructures [38]. Two types of mechanism are currently used to explain the SERS phenomenon: the electromagnetic or local field enhancement mechanism (LFEM) is a result of the enhancement of the local field from surface plasmons, and the chemical enhancement is based on the increase of the molecular polarizability. The role of the enhanced local field is to increase the Raman excitation rate of the molecule [12, 102]; therefore, LFEM is independent of the chemical nature of the molecules. The chemical mechanism, on the other hand, is sensitive to specific interactions between the adsorbed molecules and the metal surface. There are several different interactions capable of increasing the molecular polarizability; however, the formation of a resonant charge-transfer complex is the most often cited chemical SERS mechanism. The complex absorbs light at the excitation frequency producing resonance Raman scattering that appears as SERS.[102] More recently, a different SERS mechanism was proposed based on the plasmon-induced electronic coupling between the oscillating electrons in the metal and the electronic system of adsorbed molecules.[111]

When molecules bind to the metal surface, a conductive pathway is formed for the free electrons in the metal to couple with the electronic system of the molecule. Upon the excitation of plasmon resonances, the oscillating electrons in the metal penetrate into the electronic system of the adsorbed molecules causing increased molecular polarization. In this model, the plasmon resonance of the metal can be viewed as 'extending' into the adsorbed molecules causing the enhancement of the Raman scattering.

Independent of the enhancement mechanisms, SERS is a promising technique for analytical applications. One of the obstacles hindering wide analytical application of SERS relates to the development of SERS substrates that are reproducible, low cost, easy to prepare, and capable of yielding intense SERS for a variety of adsorbed molecules. This paper reports the application of low-pressure air plasma for the reduction of various silver compounds to produce SERS substrates with the required properties. Using plasma is advantageous because it provides an easy method for the fabrication of SERS substrates and the silver surface appears inherently clean for the adsorption of molecules as well as without spectroscopic background. It was previously reported that silver sulfide [112] and silver nitrate [113] can be reduced to silver metal by plasma. To the best of our knowledge, this method was not reported for SERS applications.

EXPERIMENTAL

MATERIALS

Silver (I) oxide, silver sulfate, silver nitrate, L-tryptophan, and potassium iodide were purchased from Alfa Aesar. Sodium chloride, 30% ammonium hydroxide, and 2-

propanol were received from Fisher Scientific, and 4-mercaptobenzoic acid and adenine were obtained from Sigma Aldrich. Tetramethoxysilane was purchased from Gelest, Inc. All chemicals were used as received. Deionized Millipore Milli-Q water with nominal resistivity of 18 MΩ•cm was used in all experiments. Silver chloride and silver iodide were synthesized by the addition of aqueous sodium chloride and potassium iodide, respectively, to silver nitrate solutions in dark. Silver nitrate solution was produced from the laboratory silver waste. The precipitates were washed with deionized water several times by centrifugation (Beckman J2-HS centrifuge) before drying in an oven at 100°C. Quartz slides cut to 20 x 5 x 2 mm were used as supports for the SERS substrates. Diamond particles 0.5 ± 0.25 μm were obtained from Advanced Abrasives Corporation.

INSTRUMENTATION

The Raman instrument consisted of a spectrograph (Triplemate 1377, Spex) interfaced to a liquid-nitrogen cooled CCD detector (model LN1152, Princeton Instruments,) operating at -120°C. An Innova 200 argon ion laser provided 514.5 nm excitation light focused by a cylindrical lens to a ca 0.1 x 2.0 mm spot on the sample with the total power 1.0-1.1 mW (0.5 W/cm^2). The scattered light was collected in a backscattering geometry and analyzed with 1.0 nm spectral resolution. The total acquisition time for each sample was 100 seconds. The Raman spectra were calibrated using indene. A Harrick Plasma Cleaner/Sterilizer PDC-32G was used to generate low-pressure air plasma for the reduction of the silver compounds.

RESULTS AND DISCUSSION

SUBSTRATE FABRICATION

Silver chloride (455 °C mp), silver iodide (558 °C mp), silver sulfate (600 °C mp), silver nitrate (210 °C mp), and silver (I) oxide (200 °C dec) [114] were melted on quartz slides at 50 °C higher than their respective melting temperature to make a pancake-shaped slug 1-2 mm in diameter. Glass slides were also used; however, on some slides melting of silver chloride and silver nitrate produced yellow/brown slugs whereas on quartz slides the same compounds were always colorless. For this reason, quartz slides were selected for all studies. Silver sulfate and silver (I) oxide decomposed when heated and were not studied further. The surface of the slugs was smooth and did not exhibit a porous structure as was evident from electron microscopy (images are not shown). Upon treatment with low-pressure air plasma, the slugs were reduced to silver metal porous nanostructures (Figure 6.1). Increased porosity with the treatment time was concluded based on the apparent increase of the pore size as was evident from electron microscope images obtained after 1, 3, 5, 10, 15, and 30 minutes of plasma treatment (Figure 6.2). The porous structure was formed from the reduction of the silver metal by low atomic weight ions (i.e. H, O, Ne), and the pore enlargement resulted from the sputtering of the surfaces by heavy atomic weight ions (i.e. Ar) that are present in air and ionized in the plasma.[112, 113] Additionally, all the slugs exhibited a shiny, metallic appearance after 1 minute of plasma treatment but changed to a dull appearance when the treatment was increased to 5 minutes. The dull appearance was due to the increase of the pores to the dimensions comparable and larger than the wavelength of visible light.

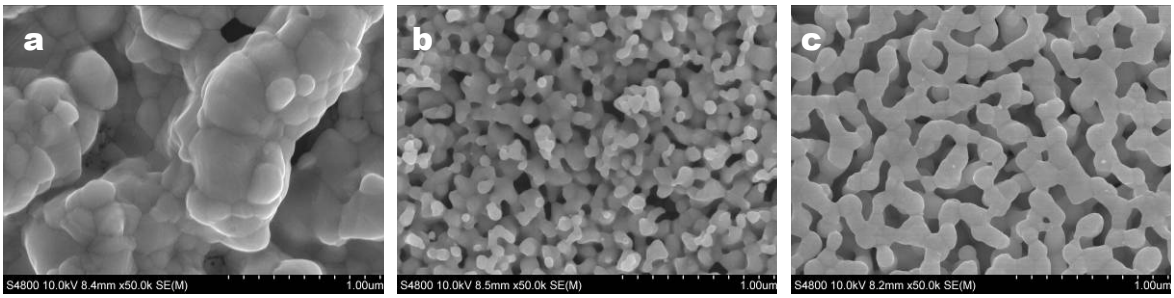

Figure 6.1. SEM images of (a) silver nitrate, (b) silver iodide, and (c) silver chloride melted on quartz and plasma treated for 5 minutes.

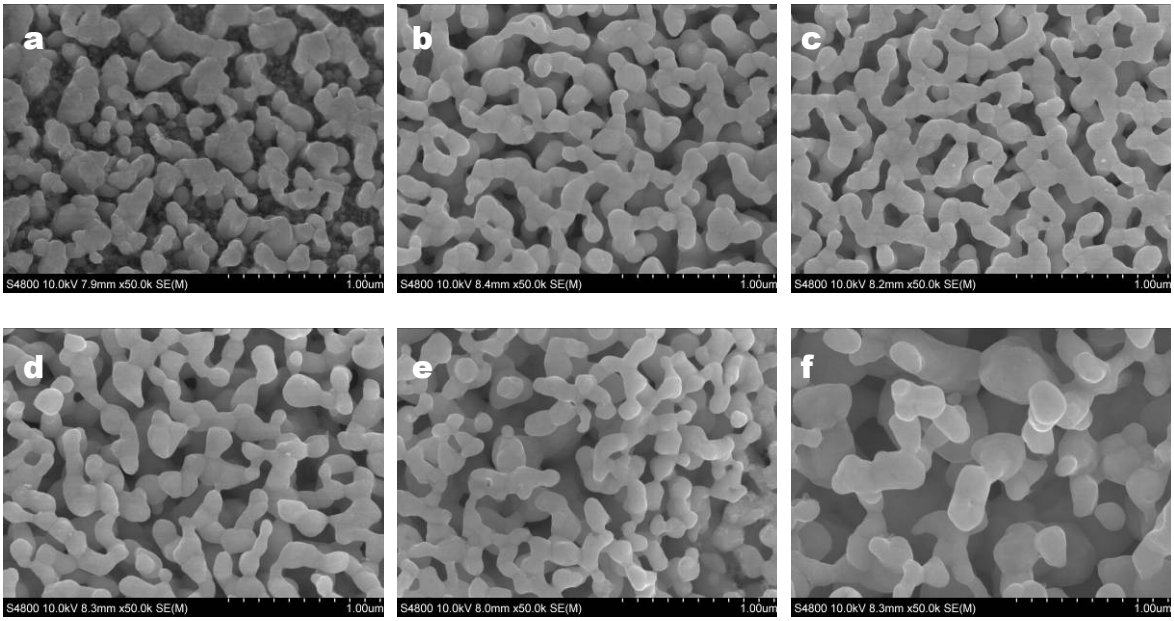

Figure 6.2. SEM images of silver chloride exposed to plasma for (a) 1, (b) 3, (c) 5, (d) 10, (e) 15, and (f) 30 minutes.

RAMAN AND ENERGY DISPERSIVE SPECTROMETRY OF SILVER COMPOUNDS

Silver chloride and silver iodide yielded no Raman bands between 500 cm^{-1} and 1700 cm^{-1} before or after the plasma treatment, whereas silver nitrate had one strong band at 1043 cm^{-1} (Figure 6.3) that corresponds to the vibration $v_1(NO_3^{-1})$.[115] This band decreased in intensity approximately 79%, 90%, and 99.7% after 1, 3, and 5 minutes of the plasma treatment, respectively. The decrease of this band intensity with time confirmed the reduction of silver nitrate to silver metal.

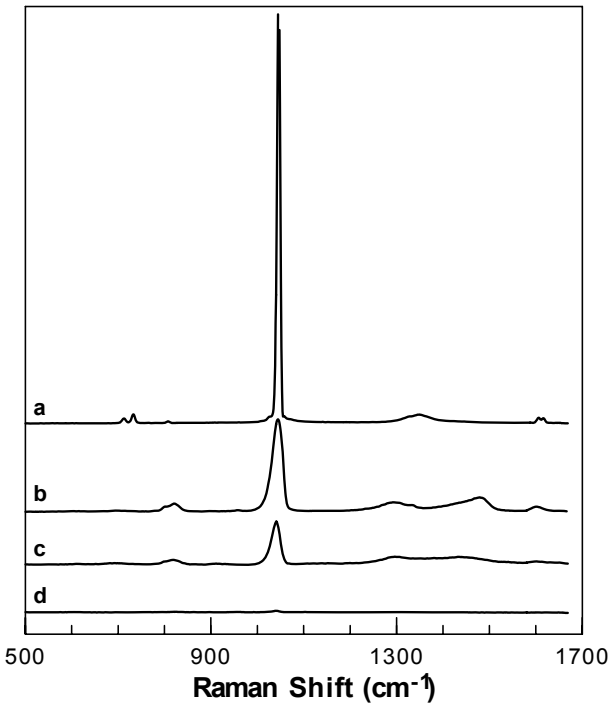

Figure 6.3. Raman spectra of silver nitrate exposed to plasma for (a) 0, (b) 1, (c) 3, and (d) 5 minutes.

As further support for the reduction of the silver compounds, the weight percent of silver chloride was measured by Energy Dispersive Spectrometry (EDS) at different plasma treatment times (Figure 6.4). The initial weight percent of silver in silver chloride was 74%, but after 1 and 5 minutes of the plasma treatment the percent increased to 94% and 99%, respectively. The similar trend was observed for silver nitrate which changed the weight percent from 37% to 91% after 5 minutes of the plasma treatment (data not shown).

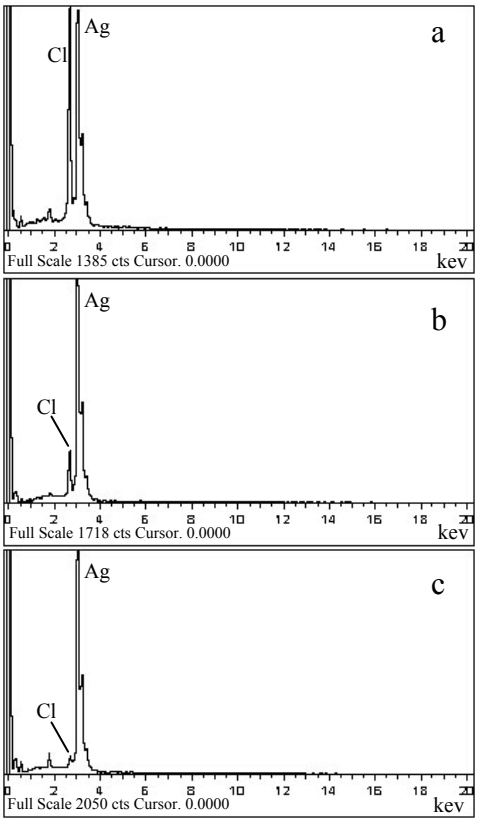

Figure 6.4. EDS spectra of silver chloride plasma treated for (a) 0, (b) 1, and (c) 5 minutes.

SURFACE ENHANCED RAMAN SCATTERING

Immediately following plasma treatment, the substrates were placed into a 1.0 x 10^{-3} M aqueous 4-mercaptobenzoic acid (4-MBA) solution for 5 minutes for SERS measurements to form a molecular monolayer. [116, 117] This model compound was selected for optimization studies of the SERS substrates. Upon placement of the substrates into the solution, it was observed that some slugs would fall off the quartz slides. Slugs produced from both silver iodide and silver nitrate were least stable in aqueous solutions; however, reduced silver chloride remained affixed to the quartz for up to 1 hour, most likely, due to its better fusion (ion exchange) of the molten silver chloride with the quartz surface during the heating process.[118, 119] No SERS studies were performed on reduced silver iodide or silver nitrate because no reproducible substrate could be produced.

Silver chloride slugs treated for 1, 2, 3, 4, 5, 8, 10, 15, and 30 minutes were used to determine the effect of the plasma treatment on SERS intensity. The strongest SERS intensity of 4-MBA was observed when plasma treatment was close to 5 minutes. The treatment for less than 4 minutes consistently produced the SERS intensity 3-5 times weaker, 8-15 minute treatments yielded 3-4 times weaker signal, and 30 minutes resulted in 5 times weaker as compared to the signal after 5 minutes of the treatment. It is thought that the strongest SERS signal that was observed after 5 minutes of the plasma treatment was due to two factors: increased surface area as well as reaching structural features in the size range (50 – 200 nm) optimum for the excitation of the efficient plasmon resonances in the visible spectral range.[34] All further experiments were performed

with the SERS substrates produced at 5 minutes of the plasma treatment. A high concentration (1.0×10^{-3} M) of 4-MBA was used in these optimization studies to ensure the saturation of the surface with the molecules. Lower concentrations could also be used but a longer exposure time was needed to reach the same SERS intensity as with the higher concentration.

Additional SERS studies were performed using adenine (1.0×10^{-5} M) and L-tryptophan (1.0×10^{-3} M) with a plasma treatment time of 5 minutes (Figure 6.5). The acquired SERS spectra showed the characteristic bands associated with each molecule with no interference from a background signal from the reduced slug. The SERS spectrum with the signal-to-noise level of 5 was measured from the reduced silver chloride slugs using 5.0×10^{-8} M adenine and 10 minute exposure time to the solution. Even though single molecule detection and concentrations in 1.0×10^{-7} M to 1.0×10^{-9} M range have been previously reported for the SERS of adenine, [120-124] the excitation powers used in those studies were 2 orders of magnitude larger than the excitation power used here.

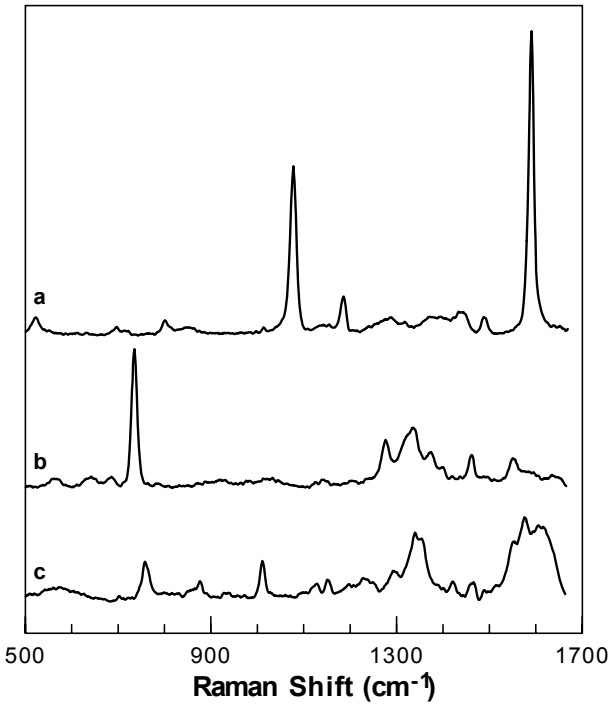

Figure 6.5. SERS spectra of (a) 4-mercaptobenzoic acid, (b) adenine, and (c) L-tryptophan on silver chloride plasma reduced for 5 minutes.

REFERENCE SIGNAL FOR SERS SUBSTRATES

The incorporation of a reference signal into the SERS substrates offered the possibility for the comparison of SERS from different molecules as well as to minimize the signal variations due to the differences in the experimental conditions. Diamond was selected to generate the reference signal because of its robustness and the presence of one narrow Raman band at 1332 cm^{-1} (Figure 6.6).[125] The fabrication of the SERS substrates with diamond is similar to the procedure described above with the addition of a 0.5 μm diamond powder to the silver chloride before melting into slugs. It was expected that incorporation of diamond powder into silver chloride followed by plasma reduction will result in a substrate that will produce strong SERS signal from molecules of interest

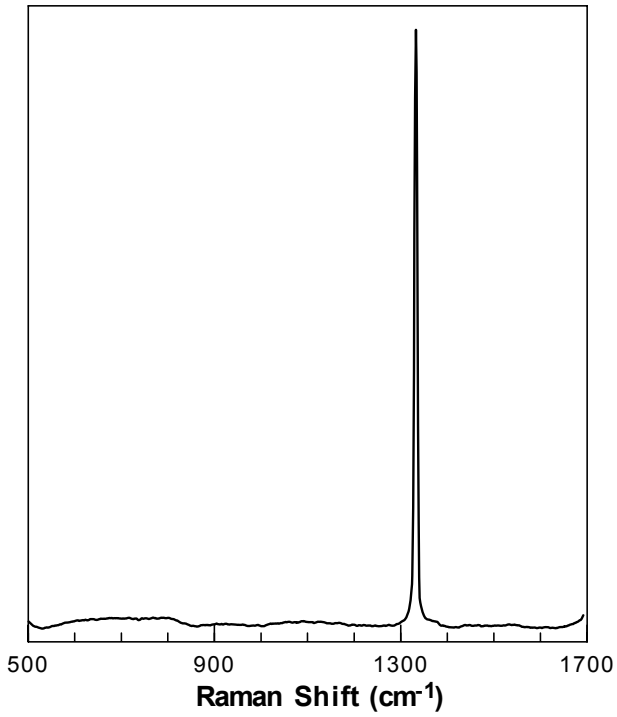

Figure 6.6. Raman spectra of diamond powder.

together with a characteristic peak due to the normal Raman scattering from diamond. No SERS phenomenon from diamond was assumed.

Upon irradiation of the SERS substrates containing diamond powder a strong Raman peak of the diamond was initially observed under experimental conditions typically used for the SERS measurements. However, the diamond signal unexpectedly decreased until it disappeared over the course of one minute under irradiation with c.a. 0.5 W/ cm^2 laser power density. This observation was especially surprising considering the perception of diamonds as being robust and chemically inert. The visual observation of the slugs revealed a black spot, most likely due to the reduced silver metal, at the location where the laser irradiated the sample. Neither silver chloride nor diamond

powder alone produced the characteristic black spot upon laser irradiation for as long as 15 minutes as well as no Raman signal degradation occurred for diamond. It was also observed that mixing the two powders in a vial and irradiating with the laser was sufficient for disappearance of the diamond Raman signal. The results were interpreted as photoreduction of silver chloride at the expense of the diamond oxidation. The oxidation product was most likely carbon dioxide gas, because no new bands were noticed in the Raman spectra that would indicate the formation of other carbonaceous species.[126-129] In addition, the plasma treatment of the diamond powder mixed with silver chloride also caused the reduction of the initial diamond peak in the Raman spectrum signifying the reduction of the silver chloride at the expense of the diamond oxidation. The plasma treatment of diamond powder alone for 5 minutes did not result in a noticeable decrease of the characteristic Raman peak.

To prevent diamond from being oxidized by silver chloride, the diamond particles were encapsulated into silica using a previously described sol-gel procedure.[17] In short, the diamond powder was suspended in a 10:1 2-propanol:water solution. Under constant stirring at room temperature, 100 μL of ammonium hydroxide was added followed by the addition of 200 μL of tetramethoxysilane. The reaction was allowed to proceed for 2 hours before washing the product with water by repeated centrifugation and drying in an oven at 100°C. Figure 7 depicts a c.a. 10 nm thick silica layer on a diamond particle.

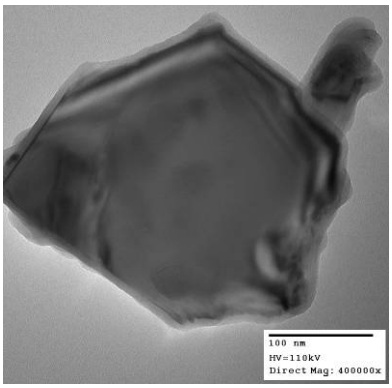

Figure 6.7. TEM image of a diamond particle coated with a 10 nm silica layer.

As expected, the encapsulated diamond particles blended to an 8% by weight mixture with silver chloride powder did not exhibit any noticeable degradation of the Raman peak upon irradiation for 10 minutes. Melting the powders together had only limited success because the 8% mixture did not form the pancake-shaped slugs or adhere to the quartz slides even after exposure to the temperature as high as 650°C. Instead, the mixture remained in a powdery form. When the amount of diamond particles was decreased to 3% by weight, the slugs were obtained; however, they were white colored with a macroscopically rough surface as opposed to clear glassy and smooth slugs when only silver chloride was used. It is also important to note that the silver chloride with 3% diamond did not melt at 505 °C (the temperature 50 °C higher than the melting point of neat silver chloride) but fused together so that the substrate would not fall off the quartz slide when immersed into liquid. The fusion produced a slug surface with the roughness that was difficult to control as opposed to melted slugs of neat silver chloride that always had a smooth surface. The later allowed introducing the roughness in a controlled way

by the plasma treatment to obtain more reproducible SERS substrates. For this reason the mass production of reproducible SERS substrates with diamond was difficult, and the SERS substrates reported here are for illustrating proof of concept that diamond can be used to generate a reference signal.

After substrates were plasma treated for 5 minutes, the diamond peak appeared weaker as compared to that before the treatment. The weakness of the diamond peak was due to fewer diamond particles exposed to the laser excitation because the diamond particles in the bulk of the slugs were 'screened' by the layer of the reduced silver metal on the surface. The SERS activity of these substrates was also reduced relative to that of substrates produced from pure silver chloride, most likely due to changes in morphology that became less favorable for the plasmon resonance excitation. Electron microscopy revealed a coarser structure of the slugs.

Plasma treated substrates containing diamond particles were exposed to a 4.2 x 10^{-4} M adenine solution for 5 minutes to test for SERS activity and spectra were acquired (Figure 8). The spectra revealed peaks from both diamond (1332 cm^{-1}) and adenine (733 cm^{-1}). The diamond peak did not change in intensity after the addition of adenine as well as it did not degrade during the measurement. The intensity of the adenine peak relative to the diamond varied within 24% between different substrates, whereas the absolute intensity of the diamond peak always stayed within 10%. The reference signal from diamond allowed absolute comparison of SERS activity between substrates and SERS signals from different molecules.

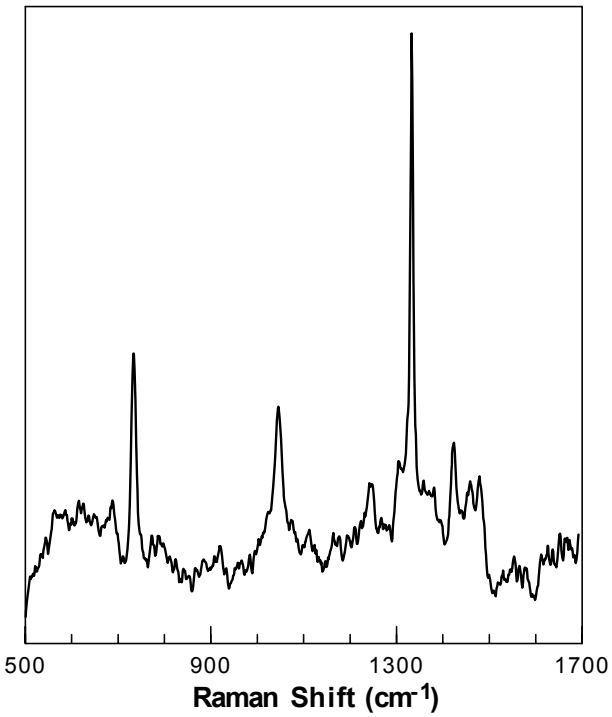

Figure 6.8. SERS spectra of adenine on plasma reduced silver chloride containing silica coated diamond nanoparticles.

CONCLUSION

Several silver compounds can be reduced to the silver metal using low-pressure air plasma. Using silver chloride, SERS-active substrates can be produced with this technique. The substrates were stable, reproducible, and free of any spectral background prior to the exposure to molecules of interest. The method is simple and can be used for rapidly producing fresh and clean SERS substrates on demand using inexpensive commonly used laboratory plasma cleaner. Additionally, the method does not employ or produce any toxic materials and the silver slugs can be recycled back into salt to make new SERS substrates. The entire process of the substrate fabrication and SERS measuring can be performed in as little as 20 min. The incorporation of diamond

particles into silver chloride powder prior to the plasma treatment provides a means for a reference signal due to the normal Raman scattering of diamond. The reference signal can be used to compare SERS activity of different substrates and SERS intensity from different molecules. However, the diamond particles should be protected to avoid photooxidation by silver chloride. The encapsulation of diamond particles in a silica shell using sol-gel chemistry is a suitable method for the protection.

CHAPTER SEVEN

CONCLUSION AND FUTURE DIRECTIONS

The effects of dielectric medium, particle size, and interparticle distance on the plasmon coupling in 2D arrays of SNPs was discussed in Chapters 2, 3, and 4, respectively. Increasing the refractive index of the medium surrounding the particles promoted the coherent plasmon coupling of the particles. Increasing the size of the particles in the 2D arrays resulted in a shift to longer wavelengths and broadening of the coupled plasmon peak. Comparison of the plasmon peak position with the particle size exhibited a linear dependence providing a straightforward correlation between the lambda maximum and particle size. Decreasing the interparticle distance resulted in spectral shifting as well as changing the intensity and sharpness of the plasmon peaks; the spectra of smaller particles shifted to longer wavelengths where as the spectra of larger particles shifted in the opposite direction upon decreasing the interparticle distance.

The effects of dielectric medium, particle size, and interparticle distance were studied separately on the 2D arrays. To obtain a complete understanding of plasmon coupling in 2D arrays, the combined effects need to be investigated. Future experiments would involve the fabrication of 2D arrays with different interparticle distances and exposing these arrays to different dielectric environments followed by measuring the visible extinction spectrum. The obtained experimental data would provide valuable information about the combined effects of dielectric medium, particle size, and interparticle distance on the plasmon coupling of 2D arrays of SNPs. Theoretical

modeling also needs to be done on the effects of particle size and interparticle distance on the plasmon coupling in 2D arrays.

One of the most promising applications of the 2D arrays of SNPs is refractive index sensors. The plasmon resonance peak position of the extinction spectra of the 2D arrays measured in the visible spectral region is sensitive to changes in the surrounding refractive index. Because the position of the peak is also sensitive to changes in the interparticle distance and particle size, optimization of the arrays needs to be performed for the ultimate goal of detecting small changes in refractive index. The performance of the optimized arrays needs to be compared with other sensors to determine their potential applicability.

Chapter 5 brought new insight into the SERS phenomenon. Even though the local field enhancement and chemical enhancement mechanisms are well established in the SERS community, they could not explain the competitive Raman enhancement observed in the studies. Plasmon-induced electronic coupling was the newly proposed SERS mechanism for molecules bonded to the silver surface. The proposed mechanism was suggested as the primary contributor but does not exclude the potential contributions from LFEM and CEM.

Understanding the SERS mechanism is critical in determining whether or not SERS can be used for the detection of different types of molecules simultaneously present in an analyte solution. The data presented in Chapter 5 suggest that SERS is a viable technique for the simultaneous detection of two different types of molecules, however, potential interferences need to be considered. The potential interferences are

evident from the fact that the intensity of the signal and the degree of quenching are dependent on the strength of the bond between the molecule and the silver metal surface. A molecule that bonds weakly to the surface may be completely quenched by another, stronger bonding molecule.

Chapter 6 is focused on the problem of SERS substrate reproducibility. Using low-pressure air plasma for the reduction of silver compounds resulted in an easy to prepare substrate with a clean silver metal surface for the bonding of molecules. The application of a diamond reference signal allowed the comparison of SERS across different substrates prepared in the same fashion. Silver chloride was found to be the best compound to make reproducible and stable SERS substrates.

The SERS substrates could be fabricated in a more reproducible manner if another method such as electrochemical deposition is used to make the silver compound layer on the supporting substrate instead of melting the salts on the surface, a somewhat crude approach. Using electrochemical deposition would make it possible to control the thickness of the compound layer. Additionally, the silica coated diamond particles could be adsorbed to the supporting substrate first followed by the electrochemical deposition of the silver compound.

APPENDICES

Appendix A

Copyright permission from American Chemical Society

American Chemical Society's Policy on Theses and Dissertations

If your university requires a signed copy of this letter see contact information below.

Thank you for your request for permission to include your paper(s) or portions of text from your paper(s) in your thesis. Permission is now automatically granted; please pay special attention to the implications paragraph below. The Copyright Subcommittee of the Joint Board/Council Committees on Publications approved the following:

> Copyright permission for published and submitted material from theses and dissertations
> ACS extends blanket permission to students to include in their theses and dissertations their own articles, or portions thereof, that have been published in ACS journals or submitted to ACS journals for publication, provided that the ACS copyright credit line is noted on the appropriate page(s).
>
> Publishing implications of electronic publication of theses and dissertation material
> Students and their mentors should be aware that posting of theses and dissertation material on the Web prior to submission of material from that thesis or dissertation to an ACS journal may affect publication in that journal. Whether Web posting is considered prior publication may be evaluated on a case-by-case basis by the journal's editor. If an ACS journal editor considers Web posting to be "prior publication", the paper will not be accepted for publication in that journal. If you intend to submit your unpublished paper to ACS for publication, check with the appropriate editor prior to posting your manuscript electronically.

If your paper has not yet been published by ACS, we have no objection to your including the text or portions of the text in your thesis/dissertation in **print and microfilm formats**; please note, however, that electronic distribution or Web posting of the unpublished paper as part of your thesis in electronic formats might jeopardize publication of your paper by ACS. Please print the following credit line on the first page of your article: "Reproduced (or 'Reproduced in part') with permission from [JOURNAL NAME], in press (or 'submitted for publication'). Unpublished work copyright [CURRENT YEAR] American Chemical Society." Include appropriate information.

If your paper has already been published by ACS and you want to include the text or portions of the text in your thesis/dissertation in **print or microfilm formats**, please print the ACS copyright credit line on the first page of your article: "Reproduced (or 'Reproduced in part') with permission from [FULL REFERENCE CITATION.] Copyright [YEAR] American Chemical Society." Include appropriate information.

Submission to a Dissertation Distributor: If you plan to submit your thesis to UMI or to another dissertation distributor, you should not include the unpublished ACS paper in your thesis if the thesis will be disseminated electronically, until ACS has published your paper. After publication of the paper by ACS, you may release the entire thesis (**not the individual ACS article by itself**) for electronic dissemination through the distributor; ACS's copyright credit line should be printed on the first page of the ACS paper.

Use on an Intranet: The inclusion of your ACS unpublished or published manuscript is permitted in your thesis in print and microfilm formats. If ACS has published your paper you may include the manuscript in your thesis on an intranet that is not publicly available. Your ACS article cannot be posted electronically on a publicly available medium (i.e. one that is not password protected), such as but not limited to, electronic archives, Internet, library server, etc. The only material from your paper that can be posted on a public electronic medium is the article abstract, figures, and tables, and you may link to the article's DOI or post the article's author-directed URL link provided by ACS. This paragraph does not pertain to the dissertation distributor paragraph above.

Questions? Call +1 202/872-4368/4367. Send e-mail to copyright@acs.org or fax to +1 202-776-8112. 10/10/03, 01/15/04, 06/07/06

Appendix B

Copyright Permission for Optical Society of America

Oct. 22. 2008 12:14PM Society for Applied Spectroscopy No. 2623 P. 1/1 of 1

10. Mark Kinnan from SAS

Victor Hutcherson

From : "Mark K Kinnan" <mkinnan@CLEMSON.EDU>
To : Office@S-A-S.org
Date : Mon, Oct-13-2008 4:56 PM
Subject : Permission to Use Content in Dissertation

Copyright Office,

I am currently preparing my dissertation and would like to include an article I authored. Please let me what I need to do in order to include text and figures from the article in my dissertation.

The article I authored is:

Kinnan, M. K.; Kumbhar, A.; Chumanov, G. Applied Spectroscopy 2008, 62, 721-726.

Thank you for your time.

Kind Regards,

Mark Kinnan

Permission granted for the use requested above:
Permission granted this 14th day of Oct 2008. Full citation required.

SAS Bonnie A. Saylor, Executive Director

REFERENCES

1. Kreibig, U. and M. Vollmer, *Optical properties of metal clusters*. 1995, Berlin ; New York: Springer.
2. Evanoff, D.D. and G. Chumanov, *Size-controlled synthesis of nanoparticles. 2. Measurement of extinction, scattering, and absorption cross sections.* Journal of Physical Chemistry B, 2004. **108**(37): p. 13957-13962.
3. Kelly, K.L., A.A. Lazarides, and G.C. Schatz, *Computational electromagnetics of metal nanoparticles and their aggregates.* Computing in Science & Engineering, 2001. **3**(4): p. 67-73.
4. Riboh, J.C., et al., *A nanoscale optical biosensor: Real-time immunoassay in physiological buffer enabled by improved nanoparticle adhesion.* Journal of Physical Chemistry B, 2003. **107**(8): p. 1772-1780.
5. Haes, A.J. and R.P. Van Duyne, *A nanoscale optical blosensor: Sensitivity and selectivity of an approach based on the localized surface plasmon resonance spectroscopy of triangular silver nanoparticles.* Journal of the American Chemical Society, 2002. **124**(35): p. 10596-10604.
6. Link, S. and M.A. El-Sayed, *Spectral properties and relaxation dynamics of surface plasmon electronic oscillations in gold and silver nanodots and nanorods.* Journal of Physical Chemistry B, 1999. **103**(40): p. 8410-8426.

7. Haynes, C.L., et al., *Nanoparticle optics: The importance of radiative dipole coupling in two-dimensional nanoparticle arrays.* Journal of Physical Chemistry B, 2003. **107**(30): p. 7337-7342.

8. Li, D.G., et al., *Simple method for preparation of cubic Ag nanoparticles and their self-assembled films.* Thin Solid Films, 2004. **460**(1-2): p. 78-82.

9. Hao, E., et al., *Optical properties of metal nanoshells.* Journal of Physical Chemistry B, 2004. **108**(4): p. 1224-1229.

10. Dirix, Y., et al., *Oriented pearl-necklace arrays of metallic nanoparticles in polymers: A new route toward polarization-dependent color filters.* Advanced Materials, 1999. **11**(3): p. 223-227.

11. Knoll, W., *Interfaces and thin films as seen by bound electromagnetic waves.* Annual Review of Physical Chemistry, 1998. **49**: p. 569-638.

12. Daniels, J.K. and G. Chumanov, *Nanoparticle-mirror sandwich substrates for surface-enhanced Raman scattering.* Journal of Physical Chemistry B, 2005. **109**(38): p. 17936-17942.

13. Freeman, R.G., et al., *Self-Assembled Metal Colloid Monolayers - an Approach to Sers Substrates.* Science, 1995. **267**(5204): p. 1629-1632.

14. Kumbhar, A.S., M.K. Kinnan, and G. Chumanov, *Multipole plasmon resonances of submicron silver particles.* Journal of the American Chemical Society, 2005. **127**(36): p. 12444-12445.

15. Evanoff, D.D. and G. Chumanov, *Size-controlled synthesis of nanoparticles. 1. "Silver-only" aqueous suspensions via hydrogen reduction.* Journal of Physical Chemistry B, 2004. **108**(37): p. 13948-13956.

16. Evanoff, D.D. and G. Chumanov, *Synthesis and optical properties of silver nanoparticles and arrays.* Chemphyschem, 2005. **6**(7): p. 1221-1231.

17. Evanoff, D.D., R.L. White, and G. Chumanov, *Measuring the distance dependence of the local electromagnetic field from silver nanoparticles.* Journal of Physical Chemistry B, 2004. **108**(5): p. 1522-1524.

18. Kelly, K.L., et al., *The optical properties of metal nanoparticles: The influence of size, shape, and dielectric environment.* Journal of Physical Chemistry B, 2003. **107**(3): p. 668-677.

19. Malynych, S. and G. Chumanov, *Light-induced coherent interactions between silver nanoparticles in two-dimensional arrays.* Journal of the American Chemical Society, 2003. **125**(10): p. 2896-2898.

20. Jensen, T.R., G.C. Schatz, and R.P. Van Duyne, *Nanosphere lithography: Surface plasmon resonance spectrum of a periodic array of silver nanoparticles by ultraviolet-visible extinction spectroscopy and electrodynamic modeling.* Journal of Physical Chemistry B, 1999. **103**(13): p. 2394-2401.

21. Sung, J., et al., *Nanoparticle spectroscopy: Dipole coupling in two-dimensional arrays of L-shaped silver nanoparticles.* Journal of Physical Chemistry C, 2007. **111**(28): p. 10368-10376.

22. Sung, J., et al., *Nanoparticle spectroscopy: Plasmon coupling in finite-sized two-dimensional arrays of cylindrical silver nanoparticles.* Journal of Physical Chemistry C, 2008. **112**(11): p. 4091-4096.

23. Felidj, N., et al., *Multipolar surface plasmon peaks on gold nanotriangles.* Journal of Chemical Physics, 2008. **128**(9): p. 094702.

24. Hicks, E.M., et al., *Controlling plasmon line shapes through diffractive coupling in linear arrays of cylindrical nanoparticles fabricated by electron beam lithography.* Nano Letters, 2005. **5**(6): p. 1065-1070.

25. Bouhelier, A., et al., *Electromagnetic interactions in plasmonic nanoparticle arrays.* Journal of Physical Chemistry B, 2005. **109**(8): p. 3195-3198.

26. Gunnarsson, L., et al., *Confined plasmons in nanofabricated single silver particle pairs: Experimental observations of strong interparticle interactions.* Journal of Physical Chemistry B, 2005. **109**(3): p. 1079-1087.

27. Gopinath, A., et al., *Photonic-plasmonic scattering resonances in deterministic aperiodic structures.* Nano Letters, 2008. **8**(8): p. 2423-2431.

28. Andersen, P.C. and K.L. Rowlen, *Brilliant optical properties of nanometric noble metal spheres, rods, and aperture arrays.* Applied Spectroscopy, 2002. **56**(5): p. 124A-135A.

29. Zou, S.L., N. Janel, and G.C. Schatz, *Silver nanoparticle array structures that produce remarkably narrow plasmon lineshapes.* Journal of Chemical Physics, 2004. **120**(23): p. 10871-10875.

30. Zou, S.L. and G.C. Schatz, *Narrow plasmonic/photonic extinction and scattering line shapes for one and two dimensional silver nanoparticle arrays.* Journal of Chemical Physics, 2004. **121**(24): p. 12606-12612.

31. Markel, V.A., *Comment on "Silver nanoparticle array structures that produce remarkably narrow plasmon line shapes" [J. Chem. Phys. 120, 10871 (2004)]*. Journal of Chemical Physics, 2005. **122**(9).

32. Atkins, P.W., *Physical chemistry*. 5th ed. 1978, New York: W. H. Freeman and Company.

33. Fleischmann, M., P.J. Hendra, and A.J. McQuillan, *Raman spectra of pyridine adsorbed at a silver electrode.* Chemical Physics Letters, 1974. **26**(2): p. 163-166.

34. Campion, A. and P. Kambhampati, *Surface-enhanced Raman scattering.* Chemical Society Reviews, 1998. **27**(4): p. 241-250.

35. Li, X.L., et al., *Self-assembled metal colloid films: Two approaches for preparing new SERS active substrates.* Langmuir, 2004. **20**(4): p. 1298-1304.

36. Seki, H., *SERS of pyridine on Ag island films prepared on a sapphire substrate.* Journal of Vacuum Science and Technology, 1981. **18**(2): p. 633-637.

37. Chumanov, G., et al., *Colloidal Metal-Films As A Substrate For Surface-Enhanced Spectroscopy.* Journal of Physical Chemistry, 1995. **99**(23): p. 9466-9471.

38. Haynes, C.L. and R.P. Van Duyne, *Plasmon-sampled surface-enhanced Raman excitation spectroscopy.* Journal of Physical Chemistry B, 2003. **107**(30): p. 7426-7433.

39. Jiang, J., et al., *Single molecule Raman spectroscopy at the junctions of large Ag nanocrystals.* Journal of Physical Chemistry B, 2003. **107**(37): p. 9964-9972.

40. Moskovits, M., *Surface-enhanced Raman spectroscopy: a brief retrospective.* Journal of Raman Spectroscopy, 2005. **36**(6-7): p. 485-496.

41. Lee, S.J., et al., *Surface-enhanced Raman spectroscopy and nanogeometry: The plasmonic origin of SERS.* Journal of Physical Chemistry C, 2007. **111**(49): p. 17985-17988.

42. Moskovits, M., *Surface-Enhanced Spectroscopy.* Reviews of Modern Physics, 1985. **57**(3): p. 783-826.

43. Gersten, J. and A. Nitzan, *Electromagnetic Theory Of Enhanced Raman-Scattering By Molecules Adsorbed On Rough Surfaces.* Journal of Chemical Physics, 1980. **73**(7): p. 3023-3037.

44. Janesko, B.G. and G.E. Scuseria, *Surface enhanced Raman optical activity of molecules on orientationally averaged substrates: Theory of electromagnetic effects.* Journal of Chemical Physics, 2006. **125**(12): p. 12.

45. Osawa, M., et al., *Charge-Transfer Resonance Esonance Raman Process In Surface-Enhanced Raman-Scattering From p-Aminothiophenol Adsorbed On Silver - Herzberg-Teller Contribution.* Journal of Physical Chemistry, 1994. **98**(48): p. 12702-12707.

46. Schatz, G.C., *Theoretical-Studies Of Surface Enhanced Raman-Scattering.* Accounts of Chemical Research, 1984. **17**(10): p. 370-376.

47. Persson, B.N.J., *On the theory of surface-enhanced Raman scattering.* Chemical Physics Letters, 1981. **82**(3): p. 561-565.

48. Otto, A., *The 'chemical' (electronic) contribution to surface-enhanced Raman scattering.* Journal of Raman Spectroscopy, 2005. **36**(6-7): p. 497-509.

49. Adrian, F.J., *Charge-Transfer Effects In Surface-Enhanced Raman-Scattering.* Journal of Chemical Physics, 1982. **77**(11): p. 5302-5314.

50. Lombardi, J.R., et al., *Charge-Transfer Theory Of Surface Enhanced Raman-Spectroscopy - Herzberg-Teller Contributions.* Journal of Chemical Physics, 1986. **84**(8): p. 4174-4180.

51. Persson, B.N.J., K. Zhao, and Z.Y. Zhang, *Chemical contribution to surface-enhanced Raman scattering.* Physical Review Letters, 2006. **96**(20): p. 4.

52. McCall, S.L. and P.M. Platzman, *Raman scattering from chemisorbed molecules at surfaces.* Physical Review B (Condensed Matter), 1980. **22**(4): p. 1660-1662.

53. Blackie, E., et al., *Bi-analyte SERS with isotopically edited dyes.* Physical Chemistry Chemical Physics, 2008. **10**(28): p. 4147-4153.

54. Goulet, P.J.G. and R.F. Aroca, *Distinguishing individual vibrational fingerprints: Single-molecule surface-enhanced resonance Raman scattering from one-to-one binary mixtures in Langmuir-Blodgett monolayers.* Analytical Chemistry, 2007. **79**(7): p. 2728-2734.

55. Etchegoin, P.G., et al., *Statistics of single-molecule surface enhanced Raman scattering signals: Fluctuation analysis with multiple analyte techniques.* Analytical Chemistry, 2007. **79**(21): p. 8411-8415.

56. Philpott, M.R., *Effect Of Surface Plasmons On Transitions In Molecules.* Journal of Chemical Physics, 1975. **62**(5): p. 1812-1817.

57. Kirtley, J.R., S.S. Jha, and J.C. Tsang, *Surface-Plasmon Model Of Surface Enhanced Raman-Scattering.* Solid State Communications, 1980. **35**(7): p. 509-512.

58. Tsang, J.C., J.R. Kirtley, and T.N. Theis, *Surface plasmon polariton contributions to strokes emission from molecular monolayers on periodic Ag surfaces* Solid State Communications, 1980. **35**(9): p. 667-670.

59. Pettinger, B., A. Tadjeddine, and D.M. Kolb, *Enhancement In Raman Intensity By Use Of Surface-Plasmons.* Chemical Physics Letters, 1979. **66**(3): p. 544-548.

60. Ting-Kuo, L. and J.L. Birman, *Quantum theory of enhanced Raman scattering by molecules on metals: Surface-plasmon mechanism for plane metal surface.* Physical Review B (Condensed Matter), 1980. **22**(12): p. 5961-5966.

61. Khizhnyakov, V. and M. Rozman, *On the theory of surface enhanced Raman scattering.* Eesti NSV Teaduste Akadeemia. Toimetised. Fuusika, Matemaatika, 1981. **30**(4): p. 349-356.

62. Chun, C., *A new theory of surface enhanced Raman scattering.* Annual Report of the Institute of Physics Academia Sinica, 1983. **13**: p. 53-56.

63. Sackmann, M., et al., *Nanostructured gold surfaces as reproducible substrates for surface-enhanced Raman spectroscopy.* Journal of Raman Spectroscopy, 2007. **38**(3): p. 277-282.

64. Abu Hatab, N.A., J.M. Oran, and M.J. Sepaniak, *Surface-enhanced Raman spectroscopy substrates created via electron beam lithography and nanotransfer printing.* Acs Nano, 2008. **2**(2): p. 377-385.

65. http://www.rta.biz., Real Time Analyzers, Sept. 1, 2008.

66. http://www.d3technologies.co.uk., D3 Technologies, Sept. 1, 2008.

67. Dirix, Y., et al., *Oriented pearl-necklace arrays of metallic nanoparticles in polymers: A new route toward polarization-dependent color filters.* Advanced Materials, 1999. **11**(3): p. 223-+.

68. Malynych, S., H. Robuck, and G. Chumanov, *Fabrication of two-dimensional assemblies of Ag nanoparticles and nanocavities in poly(dimethylsiloxane) resin.* Nano Letters, 2001. **1**(11): p. 647-649.

69. Malynych, S. and G. Chumanov, *Coupled planar silver nanoparticle arrays as refractive index sensors.* Journal of Optics a-Pure and Applied Optics, 2006. **8**(4): p. S144-S147.

70. Hong, K.M., *Multiple-scattering of electromagnetic-waves by a crowded monolayer of spheres - Application to migration imaging films.* Journal of the Optical Society of America, 1980. **70**(7): p. 821-826.

71. Kachan, S.M. and A.N. Ponyavina, *Spectral properties of close-packed monolayers consisting of metal nanospheres.* Journal of Physics-Condensed Matter, 2002. **14**(1): p. 103-111.

72. Kachan, S., O. Stenzel, and A. Ponyavina, *High-absorbing gradient multilayer coatings with silver nanoparticles.* Applied Physics B-Lasers and Optics, 2006. **84**(1-2): p. 281-287.

73. Ponyavina, A., S. Kachan, and N. Sil'vanovich, *Statistical theory of multiple scattering of waves applied to three-dimensional layered photonic crystals.* Journal of the Optical Society of America B-Optical Physics, 2004. **21**(10): p. 1866-1875.

74. Throop, G.J. and R.J. Bearman, *Numerical solutions of Percus-Yevick equation for hard-sphere potential.* Journal of Chemical Physics, 1965. **42**(7): p. 2408-2411.

75. Palik, E.D., *Handbook of Optical Constants of Solids*. Handbook of Optical Constants of Solids. 1985: Academic Press, Orlando, FL, USA

76. Jensen, T.R., et al., *Nanosphere lithography: Effect of the external dielectric medium on the surface plasmon resonance spectrum of a periodic array of sliver nanoparticles.* Journal of Physical Chemistry B, 1999. **103**(45): p. 9846-9853.

77. Novo, C., et al., *Influence of the medium refractive index on the optical properties of single gold triangular prisms on a substrate.* Journal of Physical Chemistry C, 2008. **112**(1): p. 3-7.

78. Jain, P.K., S. Eustis, and M.A. El-Sayed, *Plasmon coupling in nanorod assemblies: Optical absorption, discrete dipole approximation simulation, and exciton-coupling model.* Journal of Physical Chemistry B, 2006. **110**: p. 18243-18253.

79. Choi, B.H., et al., *Characterization of the optical properties of silver nanoparticle films.* Nanotechnology, 2007. **18**(7).

80. Sih, B.C. and M.O. Wolf, *Dielectric medium effects on collective surface plasmon coupling interactions in oligothiophene-linked gold nanoparticles.* Journal of Physical Chemistry B, 2006. **110**: p. 22298-22301.

81. Andreas, B., I. Breunig, and K. Buse, *Modeling of X-ray-induced refractive index changes in poly(methyl methacrylate).* Chemphyschem, 2005. **6**(8): p. 1544-1553.

82. Kasarova, S.N., et al., *Analysis of the dispersion of optical plastic materials.* Optical Materials, 2007. **29**(11): p. 1481-1490.

83. XiaoMing, T., et al., *Modulation of refractive index and thickness of poly(methyl methacrylate) thin films with UV irradiation and heat treatment.* Applied Surface Science, 2005. **252**(5): p. 1283-1292.

84. Gluodenis, M. and C.A. Foss, *The effect of mutual orientation on the spectra of metal nanoparticle rod-rod and rod-sphere pairs.* Journal of Physical Chemistry B, 2002. **106**(37): p. 9484-9489.

85. Kreibig, U. and M. Vollmer, *Optical properties of metal clusters*. 1995, Berlin ; New York: Springer. xx, 532 p.

86. Huang, W.Y., W. Qian, and M.A. El-Sayed, *The optically detected coherent lattice oscillations in silver and gold monolayer periodic nanoprism arrays: The effect of interparticle coupling.* Journal of Physical Chemistry B, 2005. **109**(40): p. 18881-18888.

87. Malynych, S., I. Luzinov, and G. Chumanov, *Poly(vinyl pyridine) as a universal surface modifier for immobilization of nanoparticles.* Journal of Physical Chemistry B, 2002. **106**(6): p. 1280-1285.

88. Su, K.H., et al., *Interparticle coupling effects on plasmon resonances of nanogold particles.* Nano Letters, 2003. **3**(8): p. 1087-1090.

89. Jain, P.K. and M.A. El-Sayed, *Surface plasmon coupling and its universal size scaling in metal nanostructures of complex geometry: Elongated particle pairs and nanosphere trimers.* Journal of Physical Chemistry C, 2008. **112**(13): p. 4954-4960.

90. Rechberger, W., et al., *Optical properties of two interacting gold nanoparticles.* Optics Communications, 2003. **220**(1-3): p. 137-141.

91. Olk, P., et al., *Distance dependent spectral tuning of two coupled metal nanoparticles.* Nano Letters, 2008. **8**(4): p. 1174-1178.

92. Jain, P.K., W.Y. Huang, and M.A. El-Sayed, *On the universal scaling behavior of the distance decay of plasmon coupling in metal nanoparticle pairs: A plasmon ruler equation.* Nano Letters, 2007. **7**(7): p. 2080-2088.

93. Atay, T., J.H. Song, and A.V. Nurmikko, *Strongly interacting plasmon nanoparticle pairs: From dipole-dipole interaction to conductively coupled regime.* Nano Letters, 2004. **4**(9): p. 1627-1631.

94. Pinchuk, A.O. and G.C. Schatz, *Nanoparticle optical properties: Far- and near-field electrodynamic coupling in a chain of silver spherical nanoparticles.*

Materials Science and Engineering B-Advanced Functional Solid-State Materials, 2008. **149**(3): p. 251-258.

95. Dal Negro, L., N.N. Feng, and A. Gopinath, *Electromagnetic coupling and plasmon localization in deterministic aperiodic arrays.* Journal of Optics a-Pure and Applied Optics, 2008. **10**(6): p. 10.

96. Chen, C.F., et al., *Tunable plasmonic response from alkanethiolate-stabilized gold nanoparticle superlattices: Evidence of near-field coupling.* Journal of the American Chemical Society, 2008. **130**(3): p. 824-826.

97. Lamprecht, B., et al., *Metal nanoparticle gratings: Influence of dipolar particle interaction on the plasmon resonance.* Physical Review Letters, 2000. **84**(20): p. 4721-4724.

98. Felidj, N., et al., *Grating-induced plasmon mode in gold nanoparticle arrays.* Journal of Chemical Physics, 2005. **123**(22): p. 5.

99. Kravets, V.G., F. Schedin, and A.N. Grigorenko, *Extremely narrow plasmon resonances based on diffraction coupling of localized plasmons in arrays of metallic nanoparticles.* Physical Review Letters, 2008. **101**(8): p. 4.

100. Zhao, L.L., K.L. Kelly, and G.C. Schatz, *The extinction spectra of silver nanoparticle arrays: Influence of array structure on plasmon resonance wavelength and width.* Journal of Physical Chemistry B, 2003. **107**(30): p. 7343-7350.

101. Zhang, J.T., et al., *Surface enhanced Raman scattering effects of silver colloids with different shapes.* Journal of Physical Chemistry B, 2005. **109**(25): p. 12544-12548.

102. King, F.W., R.P. Van Duyne, and G.C. Schatz, *Theory of Raman scattering by molecules adsorbed on electrode surfaces.* Journal of Chemical Physics, 1978. **69**(10): p. 4472-4481.

103. Chalmers, J.M. and P.R. Griffiths, *Handbook of vibrational spectroscopy*. 2002, New York: J. Wiley.

104. Arenas, J.F., et al., *The role of charge-transfer states of the metal-adsorbate complex in surface-enhanced Raman scattering.* Journal of Chemical Physics, 2002. **116**(16): p. 7207-7216.

105. Haynes, C.L., A.D. McFarland, and R.P. Van Duyne, *Surface-enhanced Raman spectroscopy.* Analytical Chemistry, 2005. **77**(17): p. 338A-346A.

106. Arunkumar, K.A. and E.B. Bradley, *Theory of surface enhanced Raman scattering.* Journal of Chemical Physics, 1983. **78**(6): p. 2882-2888.

107. Michaels, A.M., M. Nirmal, and L.E. Brus, *Surface enhanced Raman spectroscopy of individual rhodamine 6G molecules on large Ag nanocrystals.* Journal of the American Chemical Society, 1999. **121**(43): p. 9932-9939.

108. Giese, B. and D. McNaughton, *Surface-enhanced Raman spectroscopic and density functional theory study of adenine adsorption to silver surfaces.* Journal of Physical Chemistry B, 2002. **106**(1): p. 101-112.

109. Kim, J. and E. Ryba, *The effect of polyol OH number on the bond strength of rigid polyurethane on an aluminum substrate.* Journal of Adhesion Science and Technology, 2001. **15**: p. 1747-1762.

110. Rodgers, G.E., *Descriptive Inorganic, Coordination, and Solid-State Chemistry*. 2nd ed. 2002: Thomson Learning, Inc.

111. Kinnan, M.K. and G. Chumanov, *Surface enhanced Raman scattering from silver nanoparticle arrays on silver mirror films: Plasmon-induced electronic coupling as the enhancement mechanism.* Journal of Physical Chemistry C, 2007. **111**(49): p. 18010-18017.

112. Daniels, V., *Plasma reduction of silver tarnish on Daguerreotypes.* Studies in Conservation, 1981. **26**(2): p. 45-49.

113. Zou, J.J., Y.P. Zhang, and C.J. Liu, *Reduction of supported noble-metal ions using glow discharge plasma.* Langmuir, 2006. **22**(26): p. 11388-11394.

114. Lide, D.R., *CRC handbook of chemistry and physics, 88th Edition*. 2007, CRC Press.: Boca Raton, FL.

115. Adams, D.M. and S.K. Sharma, *Vibrational spectroscopy at high-pressures .30. Raman-study of silver, ammonium and potassium nitrates.* Journal of the Chemical Society-Faraday Transactions Ii, 1981. **77**: p. 1263-1272.

116. Michota, A. and J. Bukowska, *Surface-enhanced Raman scattering (SERS) of 4-mercaptobenzoic acid on silver and gold substrates.* Journal of Raman Spectroscopy, 2003. **34**(1): p. 21-25.

117. Lee, J.R.I., et al., *Effect of ring substitution position on the structural conformation of mercaptobenzoic acid self-assembled monolayers on Au(111).* Langmuir, 2006. **22**(26): p. 11134-11141.

118. Garfinkel, H.M., *Photochromic Glass by Silver Ion Exchange.* Applied Optics, 1968. **7**(5): p. 789.

119. Garfinkel, H.M., *Ion-Exchange Equilibria between Glass and Molten Salts.* Journal of Physical Chemistry, 1968. **72**(12): p. 4175.

120. Kneipp, K., et al., *Detection and identification of a single DNA base molecule using surface-enhanced Raman scattering (SERS).* Physical Review E, 1998. **57**(6): p. R6281-R6284.

121. Maruyama, Y., M. Ishikawa, and M. Futamata, *Surface-enhanced Raman scattering of single adenine molecules on silver colloidal particles.* Chemistry Letters, 2001(8): p. 834-835.

122. Sackmann, M. and A. Materny, *Surface enhanced Raman scattering (SERS) - a quantitative analytical tool?* Journal of Raman Spectroscopy, 2006. **37**(1-3): p. 305-310.

123. El Amri, C., M.H. Baron, and M.C. Maurel, *Adenine and RNA in mineral samples. Surface-enhanced Raman spectroscopy (SERS) for picomole detections.* Spectrochimica Acta Part a-Molecular and Biomolecular Spectroscopy, 2003. **59**(11): p. 2645-2654.

124. Lin, H.H., et al., *Surface-enhanced Raman scattering from silver-plated porous silicon.* Journal of Physical Chemistry B, 2004. **108**(31): p. 11654-11659.

125. Solin, S.A. and A.K. Ramdas, *Raman spectrum of diamond.* Physical Review B, 1970. **1**(4): p. 1687.

126. Prawer, S., et al., *The Raman spectrum of nanocrystalline diamond.* Chemical Physics Letters, 2000. **332**(1-2): p. 93-97.

127. Prawer, S., K.W. Nugent, and D.N. Jamieson, *The Raman spectrum of amorphous diamond.* Diamond and Related Materials, 1998. **7**(1): p. 106-110.

128. Ferrari, A.C. and J. Robertson, *Raman spectroscopy of amorphous, nanostructured, diamond-like carbon, and nanodiamond.* Philosophical Transactions of the Royal Society of London Series a-Mathematical Physical and Engineering Sciences, 2004. **362**(1824): p. 2477-2512.

129. Schwan, J., et al., *Raman spectroscopy on amorphous carbon films.* Journal of Applied Physics, 1996. **80**(1): p. 440-447.